

MetOp-A Reverse Engineering Study

Final Delivery

Team 5: SMB(G-S)

P. Code	Surname	Name
10913819	Albiñana Burdiel	Carlos
10882032	Aranda Romero	Fernando
10911047	Balest	Alice
10663873	Degener	Martín
10663664	Sánchez	Amanda
10620170	Scimone	Dario

Space System Engineering and Operations

Prof: M.R. Lavagna

M.Sc Space Engineering

Academic Year 2022-2023



POLITECNICO
MILANO 1863

This work is licensed under a Creative Commons “Attribution-NonCommercial-ShareAlike 4.0 International” license.



Abstract

MetOp-A is the first satellite of a series of three spacecraft, designed and built by ESA and EUMETSAT, aiming at improving the capabilities of the European weather service. This report presents a reverse engineering study aimed at defining the key parameters of the satellite. Firstly, the mission statement, high-level goals, drivers, and functions are identified to set the baseline of the analysis. Subsequently, preliminary sizing of the mission analysis and the main subsystems of the spacecraft is performed. The results of the sizings and budget estimations are presented and critically commented at the end of each chapter.

Contents

1 MetOp-A Mission	1
1.1 Mission Statement	1
1.2 High Level Goals	1
1.3 Mission Drivers	1
1.4 Functional Analysis	2
1.5 Operatonal Modes	3
1.6 ConOps	4
1.6.1 Design Reference Mission 1: DRM01 - Nominal Conditions	4
1.6.2 Design Reference Mission 2: DRM02 - Off Nominal Conditions	4
1.7 Onboard Payloads	5
1.7.1 HIRS/4 (High-resolution Infrared Radiation Sounder)	5
1.7.2 AMSU-A1/A2 (Advanced Microwave Sounding Unit)	5
1.7.3 IASI (Infrared Atmospheric Sounder Interferometer)	5
1.7.4 GOME-2 (Global Ozone Monitoring Experiment-2)	5
1.7.5 GRAS (GNSS Receiver for Atmospheric Sounding)	6
1.7.6 AVHRR/3 (Advanced Very High Resolution Radiometer)	6
1.7.7 ASCAT (Advanced Wind Scatterometer)	6
1.7.8 MHS (Microwave Humidity Sounder)	6
1.7.9 A-DCS (Advanced Data Collection System)	6
1.7.10 SEM-2 (Space Environment Monitor-2)	6
1.7.11 S&RSAT (Search&Rescue Satellite Aided Tracking System)	6
1.7.12 Instruments Characteristics	7
2 Mission Analysis	8
2.1 Launch and Early Operations Phase (LEOP)	8
2.2 Routine Operations	8
2.2.1 Objectives	8
2.2.2 Real Strategy	8
2.2.3 Modelling and Results	9
2.3 Real Mission Comparison	9
3 Propulsion Subsystem	11
3.1 System Analysis	11
3.1.1 Δv BreakDown	11
3.1.2 Architecture	12
3.2 Reverse Engineering Study	13
3.2.1 Propellant Estimation	13
3.2.2 Pressurant Estimation	14
3.2.3 Tanks Sizing	14
3.2.4 Required Thrust Level Justification	15

3.2.5	Results	15
3.3	Outputs	16
3.3.1	Configuration	16
4	Telemetry and Telecommunication Subsystem	17
4.1	TTM&TC Architecture	17
4.1.1	Data Volume Analysis	18
4.1.2	Link Budget	20
5	Attitude Determination and Control Subsystem	22
5.1	System Analysis	22
5.1.1	Architecture	22
5.1.2	Control Modes	23
5.2	Reverse Engineering	24
5.2.1	Pointing Budget	24
5.2.2	Disturbances	26
5.2.3	Slew Manoeuvres	27
5.2.4	Pointing And Desaturation	27
5.3	Outputs	27
5.3.1	Budgets	27
5.3.2	Pointing Budget	28
6	Thermal Control Subsystem	29
6.1	System Analysis	29
6.1.1	Thermal Environment	29
6.2	Reverse Engineering Study	30
6.2.1	Spacecraft	31
6.2.2	Solar Panel	32
6.2.3	Multi Nodal Analysis	33
6.3	Outputs	34
6.3.1	Results	34
6.3.2	Strategy & Configuration	34
6.3.3	Budgets	35
7	Electrical and Power Subsystem	36
7.1	System Architecture	36
7.1.1	Power Source	36
7.1.2	Reverse Engineering Sizing	36
7.1.3	Energy Storage	37
7.1.4	Power Distribution Regulation & Control	37
7.2	Budget	38
7.3	Positioning of components	39
8	Onboard Data Handling Subsystem and Configuration	40
8.1	Configuration (CONF)	40
8.1.1	Launch configuration	40
8.1.2	On-orbit configuration	41
8.2	On-Board Data Handling (OBDH)	43
8.2.1	Design	43
8.2.2	Architecture	43
8.2.3	Reverse Engineering	44
8.2.4	Outputs	47

List of Figures

1.1	Provide support functionality	2
1.2	Perform science functionality	3
1.3	Stay safe functionality	3
1.4	Overview of MetOp-A's payload module [1]	5
1.5	MetOp-A and its payloads accommodations [1]	5
2.1	Orbit maintenance strategy	9
3.1	Routine Operation Maneuvers Sequence	11
3.2	Mass estimation for Earth-orbiting satellites	13
3.3	Thrust required per number of burns	15
3.4	PS configuration [2]	16
4.1	Metop's electrical architecture [3]	18
4.2	Metop spacecraft [1]	18
4.3	Metop's Coverage with SvalSat	19
4.4	Metop's Coverage with Kiruna KAR-2	19
4.5	Coverage Time Window Histograms for SvalSat and Kiruna Ground Stations	20
5.1	Architecture of the ADCS subsystem	23
5.2	MetOp-A in orbit magnetic field	26
5.3	Simplified CAD model of MetOp-A	26
6.1	Temperature ranges of considered nodes	33
6.2	MetOp-A Artistic Representation	35
7.1	Metop-A's Electrical Architecture	36
7.2	Main bus: Unregulated 22-39 V	37
7.3	Permanent 50 V bus	37
7.4	Switched 50 V bus	37
7.5	RSJD distribution	37
7.6	Power Budget of MetOp-a	39
7.7	Solar Array stowed and deployed configuration	39
7.8	Exploded view of service module	39
8.1	MetOp-A service module and payload module	40
8.2	Available volume on the launcher [4]	41
8.3	Arianespace's PAS 1666 MVS adaptor [4]	41
8.4	Protons [4]	42
8.5	Electrons [4]	42
8.6	Service module	42
8.7	Service module OBDH architecture [5]	43
8.8	Payload module OBDH architecture [1]	43

List of Tables

1.1	Mission Change Log Table	1
1.2	Mission drivers	2
1.3	Operational modes	3
1.4	DRM01 - ConOps	4
1.5	DRM02 - ConOps	4
1.6	Instruments characteristics	7
2.1	Caption	8
2.2	Fregat Orbit separation precision [6]	8
2.3	Propellant mass budget comparison	10
3.1	PS Change Log Table	11
3.2	Monopropellant and bipropellant comparison	12
3.3	Hydrazine properties	13
3.4	Helium properties	13
3.5	Reverse Engineering Results	16
3.6	Thruster Module Configuration And Funcition [2]	16
4.1	TTMTC Change Log Table	17
4.2	TTM&TC properties	17
4.3	Link Budget	21
5.1	Sensor's redundancy	22
5.2	Actuator's characteristics	22
5.3	Nominal modes description and accuracy	25
5.4	Non-Nominal modes description and accuracy	25
5.5	Distrubance torques	26
5.6	Mass and power budget for the ADCS subsystem	28
5.7	Satellite phases pointing budget (APE)	28
6.1	TCS Change Log table	29
6.2	Heat power in different phases	29
6.3	Materials optical properties [7]	30
6.4	Components operating temperature ranges in degrees Celsius [8]	31
6.5	Installed onboard power [1]	31
6.6	Additional data	31
6.7	Nodes temperature ranges	33
6.8	Reverse engineering results	34
7.1	Instrument Power Budget	38
8.1	MA31750 specifications	44
8.2	OBC Features	46
8.3	Memory sizing	47

List of Symbols

Variable	Description	Unit	Variable	Description	Unit
a	Semi-major axis	km	B_{min}	Maximum Orbit Magnetic Field	T
α	Surface Absorptivity	-	c	Speed of Light	m/s
α_{top}	Top-Side Solar Panel Surface Absorptivity	-	C	Battery charge	Ah
α_{MLI}	Multi-Layer Insulator Surface Absorptivity	-	c_{ap}	Centre of Aerodynamic Pressure	m
γ	Heat specific ratio	-	c_d	Drag Coefficient	-
ΔP_{feed}	Feeding Line Pressure Drop	MPa	c_g	Centre of Gravity	m
ΔP_{inj}	Injector Pressure Drop	MPa	c_{sp}	Centre of Solar Pressure	m
Δv	Orbital manoeuvre cost	m/s	D	Spacecraft Residual Dipole	Am ²
Δv_{LEOP}	LEOP Orbital manoeuvre cost	m/s	D_m	Magnetotorquer Dipole	Am ²
Δv_{OP}	Routine Operation manoeuvre cost	m/s	e	Eccentricity	[$-$]
ϵ	Surface Emissivity	-	f	Acquisition Frequency	Hz
ϵ_{bottom}	Bottom-Side Solar Panel Surface Emissivity	-	F_{SC}	View Factor	-
ϵ_E	Earth Surface Emissivity	-	F_s	Solar Constant	W/m ²
ϵ_{MLI}	Multi-Layer Insulator Surface Emissivity	-	F_t	Force of Each Thruster	N
ϵ_{rad}	Radiator Surface Emissivity	-	F_{t-SK}	Thruster Force for Station Keeping	N
ϵ_{top}	Top-Side Solar Panel Surface Emissivity	-	f_{typ}	Typical Frequency	Hz
η_{pan}	Solar Panel Efficiency	-	g_0	Earth Gravity Acceleration	m/s
μ	Earth Gravitational Constant	m ³ /s ²	h	Orbit Altitude	km
ρ	Atmospheric Density	kg/m ³	h_{dist}	Disturbances Angular Momentum	Nms
ρ_{Hy}	Hydrazine Density	kg/m ³	h_m	Magnetotorquer Angular Momentum	Nms
σ	Boltzmann Constant	-	h_{RW}	Reaction Wheel Angular Momentum	Nms
σ	Deformation Strain	MPa	K_{diff}	Albedo Factor	-
θ	Maximum Deviation of the Z-axis	deg	$KIPS$	Throughput	KIPS
θ_m	Slew Manoeuvre Angle	deg	$KIPS_{fun}$	Throughput of Each Function	KIPS
A	Surface Area of the SC	m ²	$KIPS_{typ}$	Typical Throughput	KIPS
A_{cross}	Cross Area of the SC	m ²	k_{num}	Number of Components in Each Function	-
A_{rad}	Radiator Area	m ²	i	Inclination	deg
A_{pan}	Area of one side of the Solar Panel	W	I	Incidence Angle	deg
a	Earth's Albedo	-	I_{max}	Maximum Moment of Inertia	kgm ²
AKE	Absolute Knowledge Error	deg	I_{min}	Minimum Moment of Inertia	kgm ²
APE	Absolute Pointing Error	deg	I_{sp}	Specific Impulse	s
A_s	Spacecraft Surface Faces the Sun	m ²	I_v	Spacecraft Moment of Inertia	kgm ²
B	Blowdown Ratio	-	$LTAN$	Local time of ascending node	h
B_{max}	Maximum Orbit Magnetic Field	T	L_t	Thruster Moment Arm	m
			$m_{contingency}$	Contingency Mass Budget	kg

Variable	Description	Unit	Variable	Description	Unit
m_{pres}	Pressurant Mass	kg	q_0	Solar Flux	W/m^2
m_{prop}	Propellant Mass	kg	$q_{alb_{max}}$	Maximum Albedo Flux	W/m^2
m_{PS}	Propulsion Subsystem Mass	kg	q_{IR}	Infrared Flux	W/m^2
m_{p-SK}	Propellant Mass for Station Keeping	kg	q_{sun}	Solar Flux	W/m^2
m_{p-slew}	Propellant Mass for Slew Manoeuvre	kg	q	Solar Panel Reflective Coefficient	-
m_{scdry}	Spacecraft Dry Mass	kg	R	Ideal Gas Constant	Jkg/K
m_{tank}	Tank Mass	kg	RAM	Random Access Memory	Mb
$m_{thruster}$	Thruster Mass	kg	R_{orb}	Orbit Radius	km
n_{fun}	Total Number of Functions	-	SW	Swath Width	km
n_{orb}	Number of Orbits Until RW Saturation	-	T	Thrust	N
n_{slew}	Number of Slew Manoeuvres	-	T_d	Time in daylight	s
n_t	Number of Thrusters	-	T_{dist}	Disturbances Torque	Nm
Ω	Argument of perigee	deg	T_{drag}	Drag Torque	Nm
P_c	Chamber Pressure	MPa	T_e	Time in eclipse	s
Pd	Daylight power load	W	T_{gg}	Gravity Gradient Torque	Nm
Pe	Eclipse power load	W	T_m	Magnetotorquer Torque	Am^2
P_{SA}	Solar array power	W	T_{mag}	Magnetic Torque	T
P_{pres_f}	Final Pressurant Pressure	MPa	T_{orb}	Orbital Period	s
P_{pres_i}	Initial Pressurant Pressure	MPa	T_{Earth}	Earth's Temperature	K
Q_{alb}	Albedo Heat Power	W	T_{MAX}	Maximum Temperature	K
$Q_{alb_{pan}}$	Solar Panel Albedo Heat Power	W	$T_{MAX_{pan}}$	Panel Maximum Temperature	K
Q_{AVHRR}	AVHRR Heat Power	W	$T_{MAX_{RW}}$	Reaction Wheels Maximum Temperature	K
Q_{heater}	Heater Heat Power	W	T_{MIN}	Minimum Temperature	K
Q_{HIRSS}	HIRSS Heat Power	W	$T_{MIN_{pan}}$	Panel Minimum Temperature	K
$Q_{int_{MAX}}$	Maximum Internal Heat Power of the SC	W	$T_{MIN_{RW}}$	Reaction Wheels Minimum Temperature	K
$Q_{int_{MIN}}$	Minimum Internal Heat Power of the SC	W	$T_{SC_{MAX}}$	Maximum Temperature Allowed on SC	K
$Q_{int_{pan_{MAX}}}$	Maximum Internal Heat Power of the Solar Panel	W	$T_{SC_{MIN}}$	Minimum Temperature Allowed on SC	K
$Q_{int_{pan_{MIN}}}$	Minimum Internal Heat Power of the Solar Panel	W	$T_{SC_{COLD}}$	Worst Cold Case Temperature on SC	K
Q_{IR}	Infrared Heat Power	W	$T_{SC_{HOT}}$	Worst Hot Case Temperature on SC	K
$Q_{IR_{pan}}$	Solar Panel Infrared Heat Power	W	$T_{pan_{COLD}}$	Worst Cold Case Temperature on Solar Panel	K
Q_{PLM}	Payload Module Heat Power	W	$T_{pan_{HOT}}$	Worst Hot Case Maximum Temperature on Solar Panel	K
$Q_{S\&RSAT}$	S&RSAT Heat Power	W	T_{SRP}	Solar Radiation Torque	Nm
$Q_{sum_{COLD}}$	Worst Cold Case Heat Power	W	T_{tank}	Tank Temperature	K
$Q_{sum_{HOT}}$	Worst Hot Case Heat Power	W	t_b	Burning Time	s
Q_{sun}	Solar Heat Power	W	t_{cyl}	Cylindrical Tank Thickness	cm
$Q_{sun_{pan}}$	Solar Panel Solar Heat Power	W			
Q_{SVM}	Service Module Heat Power	W			

Variable	Description	Unit
$t_{eclipse}$	Eclipse Duration	s
t_{slew}	Slew Duration	s
θ	True Anomaly	deg
v	Orbital Velocity	m/s
V_{pres_f}	Final Pressurant Volume	m^3
V_{pres_i}	Initial Pressurant Volume	m^3
V_{prop}	Propellant Volume	m^3
V_{tank}	Tank Volume	L
WL	Word Length	bit/word
ROM	Read Only Memory	Mb
R_{Earth}	Earth's Mean Radius	km
r_{cyl}	Cylindrical Tank Radius	m
X_d	Daylight energy distribution efficiency	[1]
X_e	Eclipse energy distribution efficiency	[1]

Acronyms

-	Description	-	Description
ACPL	Accepted Collision Probability Level	LRPT	Low-Rate Picture Transmission
ADCS	Attitude Determination and Control Subsystem	MA	Mission Analysis
AHRPT	Advanced High-Rate Picture Transmission	MASTER	Meteoroid and Space Debris Terrestrial Environment Reference
ASCAT	Advanced Wind Scatterometer	MLI	Multi-Layer Insulator
BOL	Beginning of Life	MT	MagnetoTorquer
CAM	Coarse Acquisition Mode	NASA	National Aeronautics and Space Administration
CBS	Standard Bus Couplers	NOAA	National Oceanic and Atmospheric Administration
CCSDS	Consultative Committee for Space Data Systems	NIU	NOAA Interface Unit
CCU	Central Communication Unit	RRM	Reduction Rate Mode
CPU	Central Processing Unit	SFM	Safe Mode
CPDU	Command Pulse Direct Unit	SAS	Solar Acquisition Sensor
DBU	Digital Bus Unit	SADM	Solar Array Drive Mechanism
DES	Digital Earth Sensor	SIOV	Satellite In-Orbit Verification
DET	Direct Energy Transfer	OBC	On-Board Computer
DOD	Depth of Discharge	OBDH	Onboard Data Handling
DRAMA	Debris Risk Assessment and Mitigation Analysis	OCM	Orbit Control Mode
DSS	Digital Sun Sensor	OOP	Out Of Plane
EAIM	Intertial and Magnetic Actuators Electronics	OP	Operating Systems
EIU	Electrical Interface Unit	PAN	Solar Panel
EOL	End Of Life	PCU	Power Control Unit
ESA	European Space Agency	PDU	Power Distribution Unit
EUMETSAT	European Organisation for the Exploitation of Meteorological Satellites	PL	Payload
FoV	Field of View	PLM	Payload Module
FAM1	Fine Acquisition Mode 1	PMC	Payload Module Computer
FAM2	Fine Acquisition Mode 2	PS	Propulsion Subsystem
FAM3	Fine Acquisition Mode 3	RAAN	Right Ascension of the Ascending Node
FCM	Fine Control Mode	RBI	Remote Bus Interface
FMU	Formatting and Multiplexing Unit	RCS	Reaction Control System
FPM	Fine Pointing Mode	RSJD	Distribution and shunt junction regulator
GMAT	General Mission Analysis Tool	RTU	Remote Terminal Units
ICU	Instrument Control Unit	RW	Reaction Wheel
IP	In Plane	SC	Spacecraft
LEOP	Launch and Early Operations Phase	SFM	Safe Mode
LEO	Low Earth Orbit	SIOV	Satellite In-Orbit Verification
		SVM	Service Module
		TCS	Thermal Control Subsystem
		TTMTC	Tracking, Telemetry, Telecommand
		YSM	Yaw Steering Mode



1 | MetOp-A Mission

Change Log	
Section	Content
1.3	Page [1]; Mission Drivers justification

Table 1.1: Mission Change Log Table

1.1 Mission Statement

The MetOp program is a shared effort between the European Space Agency and EUMETSAT for a European-Based monitoring and prediction weather forecast service. Hereby is the mission statement for the MetOp-A satellite:

The Meteorological Operational Satellite Program aims to provide satellite observation and data services for weather prediction and climate monitoring. MetOp-A aims to deliver temperature and humidity profiles of the atmosphere as well as wind speed and direction above the ocean data for numerical weather prediction. Furthermore, it would be desirable (though not required) to provide data that supports Earth science research; as well as surveillance purposes

1.2 High Level Goals

Derived from the mission statement, the primary goals of the MetOp-A satellite are:

- Collect and deliver useful data to support third-party **weather forecasting systems**,
- Provide data, imagery and sounding of key elements for monitoring the **global climate**.

The secondary goals, instead, are:

- Support **Earth Science research** through relevant data,
- Provide data for **surveillance reasons**.

1.3 Mission Drivers

For the MetOp-A mission, the identified drivers are:

- **Size & On-Orbit Weight:** given the complexity and number of objectives and goals to achieve the SC, size is a key parameter to keep under control,
- **Coverage & Pointing:** since it is an Earth Observation mission, the correct coverage of the region of interest with the required precision is a crucial aspect,
- **Data Rate:** since aiming at streaming the acquired data almost in live time, this parameter is of high importance,
- **Power:** given the complexity of the system, the power requirements are expected to be critical.

More details about the selected drivers can be found in table 1.2



MetOp-A Drivers		
Driver	What limits the driver	What the driver limits
Size	Launcher selection both in terms of DV and payload bay volume, mission analysis due to high drag	Payload Size and Allocation
Coverage	Drag	Power generation, visibility window for data transmission, onboard data handling, orbit selection
Pointing	Cost, Size	Payload configuration, resolution, operation modes
Data Rate	Number of payloads, Antenna, Data Storage	OBDH, Mission Operations
Power	Size, Cost	Mission lifetime, Operation Modes
On-Orbit Weight	Launch Vehicle, Orbital	Mission lifetime, Operation modes, Payload Weight

Table 1.2: Mission drivers

1.4 Functional Analysis

To define the functionalities that MetOp-A satellite must fulfill, a first breakdown is performed to identify the main players of the mission:

- Launch Segment,
- Space Segment,
- Ground Segment.

The Launch Segment will be analyzed at a later stage, the ground segment is tasked with data analysis and distribution, while for the space segment three main functionalities are identified:

- Provide Support,
- Perform Science,
- Stay Safe.

Those functionalities are further decomposed in the figure below.

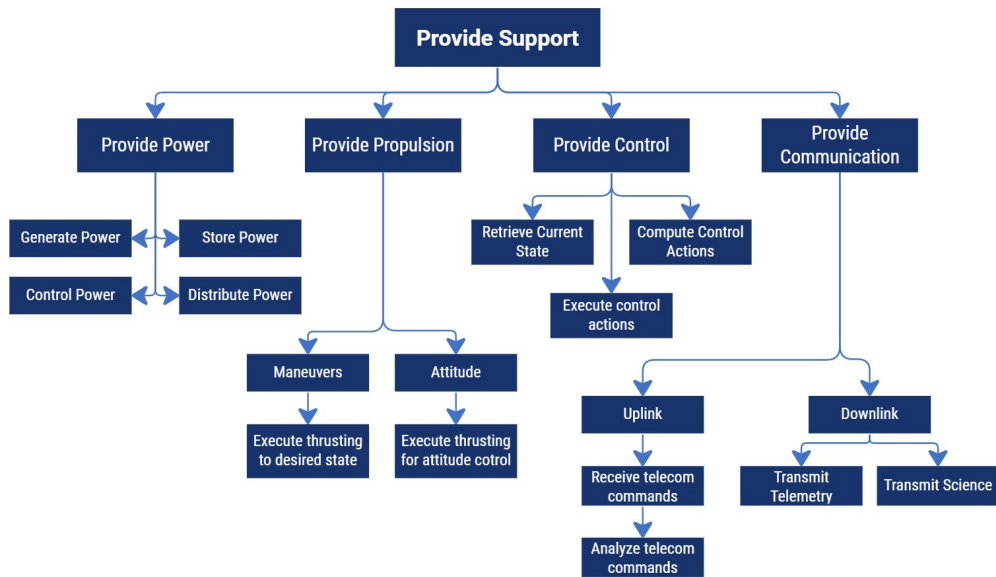


Figure 1.1: Provide support functionality

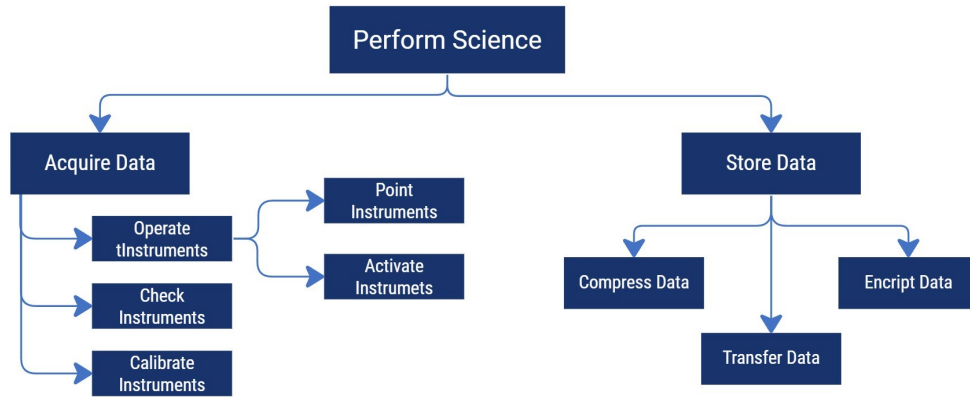


Figure 1.2: Perform science functionality

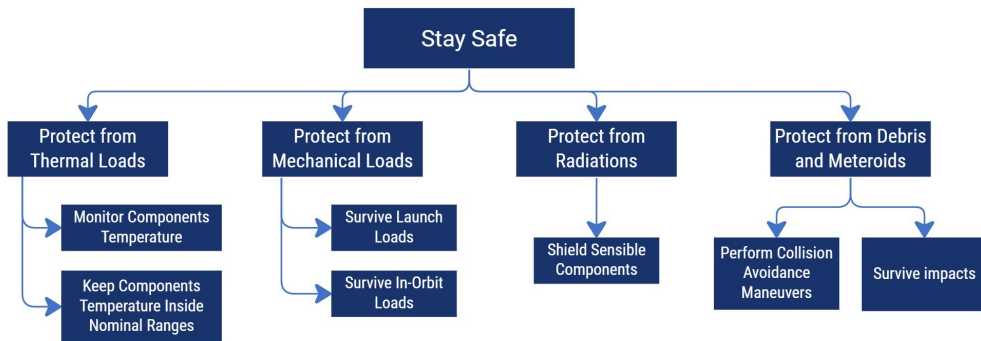


Figure 1.3: Stay safe functionality

1.5 Operational Modes

MetOp-A Operational Modes	
Mode	Description
Science	All Payloads point to Nadir
Communication	Tracking Telemetry and Telecommand via S-Band Antenna
Science Transmission	Point to Nadir and transmit science data via X-Band antenna and/or AHRPT/LRPT
Power Generation	Solar Panel Pointed to the Sun
Sleep	All instruments off, minimum systems active
Safe	Sun-pointing [3] power positive, thermally stable, establish comms, minimal operations
Thrusting	PS active, fine pointing

Table 1.3: Operational modes



1.6 ConOps

1.6.1 Design Reference Mission 1: DRM01 - Nominal Conditions

DRM01 - ConOps	
Phase	Description
LEOP	<ol style="list-style-type: none">1. Satellite deployed from the launcher,2. Platform activation,3. Acquire state and perform detumbling,4. System check and telemetry transfer to ground,5. Deploy solar panel,6. Deploy appendices,7. Transfer to operational orbit
SIOV [9]	<ol style="list-style-type: none">1. Telecommands received from ground to begin phase,2. Switch on all the payloads3. Command the payloads and check their telemetry,4. Start acquiring scientific data,5. Begin X-Band data transmission,6. Stop X-Band data transmission,7. Begin High/Low-Resolution Picture Transmission,8. Stop High/Low-Resolution Picture Transmission,9. Stop acquiring scientific data.
Science Acquisition	<ol style="list-style-type: none">1. Telecommands received from ground to begin phase,2. Exit sleep mode,3. Perform system check,4. Power generation if required,5. Activate instruments,6. Activate 3-Axis stabilization and point instruments to Nadir,7. Acquire, process and store data,8. Downlink data,9. Enter sleep mode.
Disposal	<ol style="list-style-type: none">1. Telecommands received from ground to begin phase,2. Execute disposal burn,3. Passivate systems,4. Reenter atmosphere.

Table 1.4: DRM01 - ConOps

1.6.2 Design Reference Mission 2: DRM02 - Off Nominal Conditions

DRM02 - ConOps	
Phase	Description
Off-Nominal	<ol style="list-style-type: none">1. System check has identified off-nominal conditions,2. Add off-nominal conditions identified to downlink,3. If risk criteria are met → Enter Safe Mode4. If risk criteria are not met → Await for Ground

Table 1.5: DRM02 - ConOps



1.7 Onboard Payloads

The MetOp-a satellite payload module consists in 11 instruments, mounted on the external panels for the collection of scientific data for weather forecasting and for the monitoring of the global climate. [1]



Figure 1.4: Overview of MetOp-A's payload module [1]

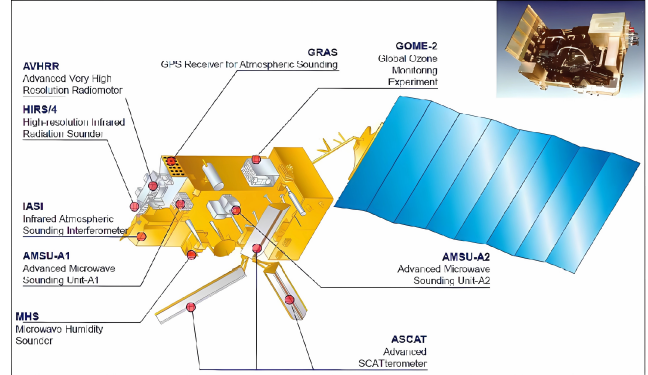


Figure 1.5: MetOp-A and its payloads accommodations [1]

1.7.1 HIRS/4 (High-resolution Infrared Radiation Sounder)

HIRS/4 is an across-scanning system, that measures the incident radiation primarily in the infrared and visible regions of the spectrum. The instrument is composed by a telescope and a rotating wheel with different filters. This allows to obtain temperature profiles, moisture content, cloud height and surface albedo. The instrument measures with different sensors the longwave (6.5 to 15 μm), shortwave (3.7 to 4.6 μm) and visible (0.69 μm) regions. [1] [10]

1.7.2 AMSU-A1/A2 (Advanced Microwave Sounding Unit)

AMSU-A1/A2 are two microwave radiometers that measure the oxygen absorption bands, for global atmospheric temperature sounding, and to provide information on atmospheric water. These across-scanning systems measure in fifteen spectral bands, the two lowest frequencies are measured by AMSU-A1 while the rest are perceived by AMSU-A2. Each device has the following modules: a receiver, a signal processor, a structural/thermal subsystem and an antenna. Data from AMSU-A is used in conjunction with the data from HIRS to retrieve scientific information. [1] [11] [10]

1.7.3 IASI (Infrared Atmospheric Sounder Interferometer)

IASI is designed to measure atmospheric spectra in the infrared, providing an atmospheric emission spectrum (with high vertical resolution) for meteorologists to derive temperature and humidity. The system permits the characterization of cloudiness as well as trace gases, such as: ozone profiles and columnar amounts of carbon monoxide (CO), carbon dioxide (CO₂), nitrous oxide (N₂O), and methane (CH₄), crucial to monitor the greenhouse effect. The instrument is composed by a management unit (sensor module) and a digital processing subsystem which performs the inverse Fourier transform (Fourier transform spectrometer), with an associated infrared imager, and the radiometric calibration. [1]

1.7.4 GOME-2 (Global Ozone Monitoring Experiment-2)

GOME-2 is a medium resolution and cross-track scanning spectrometer, able to measure the solar radiation transmitted or scattered from the Earth's atmosphere/surface. It consists of a double grating spectrometer, a polarizing monitoring unit, the focal-plane assembly, a scan unit, a command and data handling unit and a calibrating unit. Its main objectives are the measurement of total column amount of various gases (water (H₂O), nitrogen dioxide (NO₂), chlorine dioxide (OCIO), bromine monoxide (BrO), hypochlorite (ClO) and pollutants like sulfur dioxide (SO₂) and formaldehyde (HCHO)), as well as the stratospheric and tropospheric profiles of the ozone, which are a useful indicator of the evolution of the global climate. [1]



1.7.5 GRAS (GNSS Receiver for Atmospheric Sounding)

GRAS provides atmospheric temperature and humidity profiles. It's composed of three antennas, pointing in the satellite's velocity, anti-velocity, and zenith directions; three radio frequency conditioning units; and an electronic unit. Since the refractive index of the atmosphere depends upon the pressure, temperature and humidity, it measures the microwave signals passing through, to get a profile of those parameters. In addition, GRAS can provide the height of the tropopause with a vertical accuracy of < 1 km. [1]

1.7.6 AVHRR/3 (Advanced Very High Resolution Radiometer)

The AVHRR is an imaging radiometer that detects energy in the visible and infrared regions of the spectrum. It consists of a scanner module, an electronic module, an electronic calibration, a radiant cooler module, an optical sub-system, and a baseplate unit. The instrument measures reflected solar energy and radiated thermal energy from land, sea, clouds, and the intervening atmosphere. Providing radiance data for investigation of clouds, land-water boundaries, snow and ice extent, ice or snow melt inception, day and night cloud distribution, temperatures of radiating surfaces, sea surface temperature and vegetation classification and greenness. [1] [12] [13]

1.7.7 ASCAT (Advanced Wind Scatterometer)

ASCAT determines wind vector fields at sea surface, as well as monitoring of snow and ice distribution over land and sea. By sequentially illuminating two strips of the sea surface, the instrument allows a fast global coverage of the Earth's surface. The device consists of six antennas, the scatterometer front end, a radio frequency unit, a high power amplifier, a digital processing unit, a power distribution unit, and an instrument control unit. Displayed as follows: three antennas are employed for each of the two swaths to obtain the wind speed and direction measurements. The other three are located sideward at 90°, forward at 45° and afterward at 135°. [1]

1.7.8 MHS (Microwave Humidity Sounder)

MHS is a radiometer designed to scan the atmosphere, to measure the apparent upwelling microwave radiation from the Earth. It provides a detailed picture of the atmospheric humidity, useful for weather prediction models and weather forecasting. This device consists of a scan mechanism, a receiver, and a control electronics unit. It works in conjunction with AMSU-A1/A2, AVHRR/3 and HIRS/4. [1] [14]

1.7.9 A-DCS (Advanced Data Collection System)

A-DCS is designed to collect and distribute scientific data, useful for studying oceans, volcanoes, and wildfires, among others. It aims to gather information and location from ground segments, dedicated to environmental data measurement. It specifically provides measurements of temperature, pressure, humidity, sea levels and location, with a worldwide coverage. The system is composed by a receiver processing unit, a control unit, a telemetry encoder and memory, a data recovery unit, and a transmitter. [1]

1.7.10 SEM-2 (Space Environment Monitor-2)

SEM-2 is a spectrometer that provides measurements of the flux of charged particles, to determine the intensity of the Earth's radiation belts, as well as knowledge on solar terrestrial phenomena and solar wind warnings. These anomalies could impair the nominal operations of satellites. SEM-2 has three major components: the total energy detector, the medium energy proton and electron detector, and a data processing unit. [1] [15]

1.7.11 S&RSAT (Search&Rescue Satellite Aided Tracking System)

S&RSAT is part of an international cooperative satellite-based radiolocation system (COSPAS-S&RSAT) to support search and rescue operations for aviators, mariners, and land travelers in distress. It is composed by a repeater and a processor. [1] [16]



1.7.12 Instruments Characteristics

Table 1.6 outlines the characteristics of each payload and links them to the mission goals they fulfil. Goal 1 (G1) refers to weather forecasting data, G2 to global climate monitoring, G3 to data supporting Earth Science research, and G4 to surveillance.

Instrument	Weight [kg]	Power Consumption [W]	Data Rate [kbit/s]	G1	G2	G3	G4
HIRS/4	35	24	2.88	X	X	X	
AMSU-A	104	99	3.2	X	X	X	
IASI	236	210	1500	X	X	X	
GOME-2	73	42	400	X	X		
GRAS	30	30	27	X	X		
AVHRR/3	33	27	621.3	X	X	X	
ASCAT	260	215	42	X	X	X	
MHS	63	< 93	3.9	X	X		
A-DCS	30	72	0.4-4.8	X	X	X	X
SEM-2	18	10	160		X	X	
S&RSAT	51.5	86	2.4				X

Table 1.6: Instruments characteristics



2 | Mission Analysis

Change Log	
Section	Content
2.2.3	Page [9] ; Consistency with Propulsion Subsystem

Table 2.1: Caption

2.1 Launch and Early Operations Phase (LEOP)

LEOP stage of the mission is handled by ESA/ESOC after Soyuz Launcher and Fregat Upper stage delivery. After three days of LEOP, Hand-Over to EUMESTAT is performed. In this period, the delivery orbit must be corrected such that after two weeks a drift stop manoeuvre can leave MetOp-A in its final reference orbit [6]. Fregat's separation orbit precision is noted in Table 2.2.

Deviation from desired orbit is assessed by OD&C team on ground and a manoeuvre plan is devised. The satellite shall perform OOP and IP burns to modify the Keplerian elements, out of which the most costly is the inclination change by means of an OOP manoeuvre. OOP burns are not in a single node crossing, but divided into two burns at both nodes for increased precision. Also, MetOp-A is not able to perform a single burn of 0.12 deg inclination change [6]. However, as a first approximation for fuel estimation, a plane change of 0.12 deg in a circular orbit of altitude 817 km results in a Δv cost of 46 m/s. The 22N hydrazine mono-propellant thrusters used for orbit control have an Isp between 220 and 230 s [17] [18], resulting in a propellant usage of around 85 kg in the worst case scenario.

Parameter	$3 - \sigma$
a [km]	± 12
e [-]	± 0.001
i [deg]	± 0.12
RAAN [deg]	± 0.12
ω [deg]	± 12

Table 2.2: Fregat Orbit separation precision [6]

2.2 Routine Operations

2.2.1 Objectives

The main objectives of the operational phase regarding MA were [19]:

- Maintenance of the Local Time of Ascending Node (LTAN) within 2 minutes around 21:30. Imposed to satisfy the sun-calibration geometrical needs for the GOME payload.
- Maintaining the repeat orbit within 5 km around the nominal ground track and achieving frozen eccentricity (e), ensuring optimal observation conditions for calibration and operation of the instruments, especially ASCAT.

The orbit maintenance strategy is clearly correlated with the Science Acquisition phase described in section (Con-Ops). It is meant to achieve the perfect conditions for information acquisition and transmission, ensuring the proper functioning and operation of all the payloads.

2.2.2 Real Strategy

To fulfil these strict requirements, more than 95% of the fuel budget was foreseen for orbit maintenance, while the remaining was used for attitude control [19].

The orbit maintenance strategy defined during the design phase consisted of:

- Performing Out Of Plane (OOP) manoeuvres to conserve the proper inclination (I), 98.7 deg, of the orbit. This parameter is strictly related to the LTAN maintenance and, due to their nature, this type of manoeuvres is the one with the highest cost.



- Performing In Plane (IP) manoeuvres, after the OOP, to ensure the frozen eccentricity and the repeat orbit objectives. As there is no plane orbit plane inclination these manoeuvres were meant to be less costly.

The two steps manoeuvre explained above was planned to be performed every 18 months of operation. This range was imposed by the expected inclination variation with time. Figure 2.1 shows this pre-calculated variation. As can be seen, inclination keeps decreasing with time while the LTAN has a concave behaviour. The set of manoeuvres is placed at a time when the Local Time of Ascending Node would get closer to the required limits.

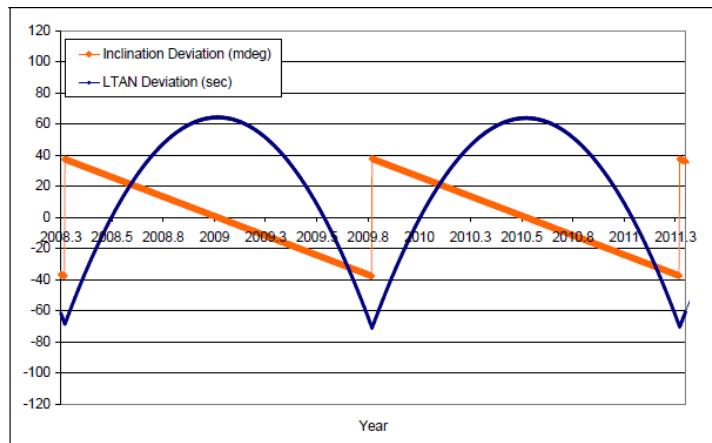


Figure 2.1: Orbit maintenance strategy

Due to the location of the thrusters on board, the Metop platform had the need to rotate the spacecraft around the yaw axis before performing the OOP. Moreover, the instruments' illumination conditions imposed that the manoeuvres were done during eclipse time [20]. These special circumstances made more difficult the orbit maintenance strategy as the manoeuvre time was short and dependent on the epoch. Actually, more than one manoeuvre was usually needed to achieve the desired inclination.

2.2.3 Modelling and Results

For modelling the operational phase, GMAT software. The initial conditions for the propagation are the ones achieved after the LEOP phase. In this case, the first transmitted orbital data, on the 22nd of October 2006, is employed in the propagator [6].

A simplified procedure is applied for the simulation. First, it is considered that there is no need to slewing the spacecraft to appropriately position the thrusters. Besides, the necessity of having the manoeuvre during eclipses is not considered in the calculations. Considering the mission lifespan a total of three orbit maintenance manoeuvres should be done, including both OOP and IP. Regarding the margins, as it is a planned orbit maintenance strategy, deterministic, either a 5% or 10 m/s shall be applied.

Station Keeping Δv budget consists of 3 burns of 12 m/s each. As the total margin from the 5% rule is less than 10 m/s, this last value must be applied to the overall Δv . Therefore, the total budget coming from the Operational Phase is:

$$\Delta v_{OP} = 36 + 10 = 46 \text{ m/s}$$

2.3 Real Mission Comparison

Propellant Mass Budget attained from reverse Engineering the MetOp-A mission yields in comparable values. As seen in section 2.1, LEOP mass budget is a worst case scenario calculation. Actual inclination deviation was of 40 mdeg and 4.8 km above reference semi-major axis results, indicating good injection orbit parameters from Fregat Upper stage resulting in small corrective manoeuvres.



	Real Estimation	Used	Reverse Analysis
LEOP	60	14	21.8
Routine Operation	100	94.7(2014)	46

Table 2.3: Propellant mass budget comparison

Regarding the routine operations, the reversed Δv is quite similar with respect to the designed one. In fact, the relative error between the two of them is 9%, a good value considering the simplifications assumed for the estimation. Nevertheless, the real used propellant mass is much less, with a weight of 94.7 kg in 2014. This is due to the optimisation of the orbit maintenance strategy after performing the first OOP manoeuvre in 2008. ESA experts noticed that the first designed plan was not efficient as the plane change was too expensive in terms of propellant. A new strategy was designed and applied in 2009 generating a lower propellant consumption [19].



3 | Propulsion Subsystem

Change Log	
Section	Content
3.1.2.2	Page [13]; Pressurant choice justification
3.2.1	Page [14]; I_{sp} justification
3.2.2	Page [14]; Blow-down ratio and chamber pressure justification

Table 3.1: PS Change Log Table

3.1 System Analysis

Developed and produced by ESA and EUMETSAT, MetOp-A is the first of three large spacecrafts carrying eleven scientific instruments to the LEO region for meteorological prediction purposes. The design of the Propulsion Subsystem is, therefore, heavily influenced by the following drivers:

- **Safety:** being the first satellite of the program, limited knowledge of the system is available. This translates into high safety margins - specifically on the loaded propellant mass - and on a high level of redundancy,
- **Complexity:** given the already high complexity of the PLM, the design process of the PS focuses on obtaining the optimal configuration with the simplest solution achievable.

3.1.1 Δv BreakDown

MetOp-A's nominal mission can be split, from a maneuvering point of view, into two main phases: LEOP and Routine Operations.

The first one has the aim of correcting the launcher orbit dispersion. It starts after the spacecraft's separation from Fregat Upper Stage and consists of OOP and IP series of burns. The fuel consumption for LEOP is estimated to be $\Delta v_{LEOP} = 21.8 \text{ m/s}^1$, margins included.

While on Routine Operation, a series of orbit maintenance burns are performed to keep the satellite in its nominal operating region. Specifically, two types of maneuvers are planned:

- **Out-Of-Plane:** the OOP burn aims to correct the orbit inclination, keeping it close to an SSO, thus limiting the LTAN drift from the nominal value. This maneuver is the most expensive and produces a variation of eccentricity due to thruster misalignment with respect to the satellite frame,
- **In-Plane:** IP burn is required to correct the eccentricity change produced by the OOP as per frozen eccentricity requirement imposed by the ASCAT instrument.

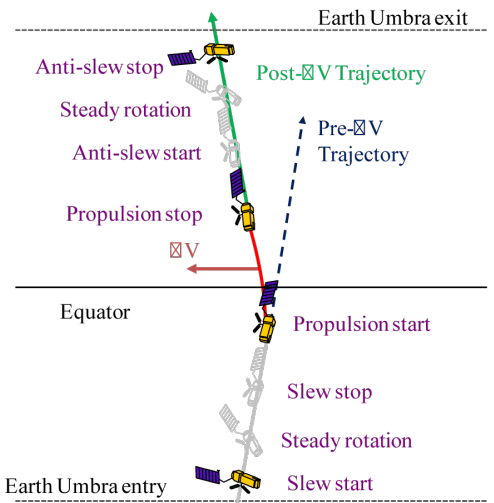


Figure 3.1: Routine Operation Maneuvers Sequence

¹revised value with respect to first assignment delivery



Due to thrusters' positioning, two slew maneuvers are required: first to align the engines with the perpendicular to velocity direction and then to reorient the spacecraft for science acquisition. Moreover, both maneuvers must be carried out in eclipse conditions to protect the scientific instruments from exposure to the Sun when the spacecraft is performing the slew and the anti-slew. These two conditions play a significant role in the scheduling of the burns as well as in the number of engines selected. The budget for the Routine Operation is $\Delta v_{OP} = 46$ m/s¹ considering a set of three maneuvers of $\Delta v = 12$ m/s each plus 10 m/s margin.

In addition to nominal phases, a contingency condition is included into the mission's budget, aiming to keep the spacecraft in a safe attitude and then reacquire the operational state once the anomaly is solved. 30 kg per year [17] are therefore added to the nominal propellant mass budget.

Lastly, it must be noted that no Δv budget is allocated for De-Orbiting since no EOL strategy was foreseen at the time of the design.

3.1.2 Architecture

3.1.2.1 Propellant Type

When designing an in-space propulsion system, a set of options are available:

- Cold Gas,
- Monopropellant,
- Bipropellant,
- Electric.

In the case of the MetOp-A mission, Cold Gas and Electric are discarded a priori since the level of thrust provided by those technologies is incompatible with the mission's needs, specifically with the OOP maneuver. Moreover, at the time of the design, electric propulsion was not mature enough to guarantee a high level of reliability.

The choice is, therefore, either a monopropellant system or a bipropellant one. Table 3.2 shows both pros and cons.

	Pros	Cons
Monopropellant	<ol style="list-style-type: none">1. Simple system2. Good for attitude control3. Restartable4. Throttles	<ol style="list-style-type: none">1. Cannot reach high thrust2. Extra power needed for catalyst bed heating
Bipropellant	<ol style="list-style-type: none">1. Higher specific impulse2. High thrust3. Restartable	<ol style="list-style-type: none">1. Complex system2. Difficult to throttle

Table 3.2: Monopropellant and bipropellant comparison

From a performance viewpoint, combining the two technologies is the optimal solution. Specifically, using monopropellant thrusters for attitude control and bipropellant to carry out the orbit maintenance maneuvers. However, the resulting complexity would be very high, requiring the development of two parallel systems.

Thus, keeping in mind the drivers stated in section 3.1, the optimal solution is found to be the employment of a monopropellant-only propulsion subsystem. The downside of this choice is the splitting of the orbit maintenance maneuvers into multiple takes since the available thrust levels don't allow for a single-take solution, due to section



3.1.1 constraints.

The selected propellant is Hydrazine, given its wide utilization in space propulsion systems, high performance, and stability. Nevertheless, the high freezing point is a parameter to keep under control when designing the Thermal Control Subsystem. Hydrazine properties are listed in table 3.3

Formula	Density	Freezing Point	Boiling Point
N_2H_4	$1.008 \cdot 10^3 \text{ kg/m}^3$	274.7 K	386.8 K

Table 3.3: Hydrazine properties

3.1.2.2 Feeding System

For the feeding system selection, the choice relies on two main options: Blowdown or Pressure Regulated. The latter allows constant pressure in the system, which translates into higher precision and performance; the downside is the need for dedicated tanks and more regulation components, thus more complexity. For this reason, a Blowdown solution is chosen, guaranteeing higher simplicity and reliability despite entailing a decrease in the level of thrust throughout the mission's lifetime.

For the choice of the pressurant gas, two main options are available: Helium and Nitrogen. The first one offers low molar mass and it's stable with Hydrazine but at the same time is prone to leakages. The former is not susceptible to leakages while having higher molar mass and reaction issues with Hydrazine. The final selection lead to the usage of Helium given its compatibility and performances, specific pre-flight checks are needed to look for possible leaks. Helium properties are listed in table 3.4

Formula	Density	γ	R
He	$0.125 \cdot 10^3 \text{ kg/m}^3$	1.67	277.3 Jkg/K

Table 3.4: Helium properties

3.2 Reverse Engineering Study

3.2.1 Propellant Estimation

To compute the propellant mass required to carry out the operational life of MetOp-A, a first estimation of the spacecraft's in-orbit dry mass is performed by using statistical data coming from past missions.

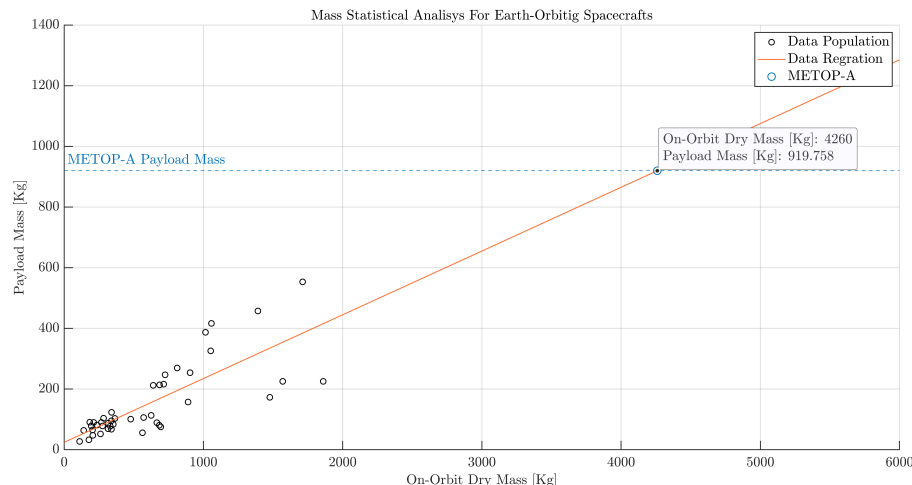


Figure 3.2: Mass estimation for Earth-orbiting satellites



The result is reported in table 3.5. As can be seen from fig 3.2, the majority of the available points are located in the lower range of payload mass, thus producing an overestimation of the spacecraft's one compared to the real data, that will reflect on an overestimation of the following masses and volumes. The wet mass is then retrieved using the Rocket Equation - with $I_{sp} = 230\text{ s}$ [8]- and then by adding the budget for contingency operations.

$$m_{sc_{wet}} = m_{sc_{dry}} \cdot e^{\frac{\Delta v}{I_{sp} \cdot g_0}} + m_{contingency} \quad (3.1)$$

The required propellant is computed using equation 3.2, with the following margins: 2% for propellant residuals, 0.5% for loading uncertainty and 3% for ullages [21], and a 10% as the preliminary budget for the ADCS [22].

$$m_{prop} = ((m_{sc_{wet}} - m_{sc_{dry}}) + 5.5\%) + 10\% \quad (3.2)$$

Lastly, equation 3.3 gives the required volume for the propellant.

$$V_{prop} = \frac{m_{prop}}{\rho_{Hy}} + 10\% \quad (3.3)$$

3.2.2 Pressurant Estimation

Once the properties of the propellant are known, the pressurant's parameters are retrieved. The initial volume of Helium is computed through 3.4, by fixing the blow-down ratio to $B = 4.45$ - a good assumption for a preliminary analysis [8] - and by assuming the transformation to be isothermal.

$$V_{pres_i} = \frac{V_{prop}}{B - 1} \quad (3.4)$$

In the worst case scenario the final pressure of the pressurant must be at least equal to the final pressure of the tank, which is calculated as:

$$P_{pres_f} = P_c + \Delta P_{inj} + \Delta P_{feed} \quad (3.5)$$

where P_c is set to 50 Bar - a middle value of the range given for a blow-down system in [8] -, ΔP_{inj} is usually 30% of P_c and ΔP_{feed} is typically set to 500 Bar [8]. To retrieve the initial volume of the pressurant 3.7, the final pressure of Helium is needed; it is computed by reversing the blow-down ratio's equation as it follows:

$$P_{pres_i} = B \cdot P_{pres_f} \quad (3.6) \qquad V_{pres_f} = \frac{P_{pres_i} \cdot V_{pres_i}}{P_{pres_f}} \quad (3.7)$$

Finally, the mass of the pressurant is computed as in 3.8 where $T_{tank} = 293\text{ K}$ [8]. A 20% margin is added in compliance to MAR-MAS-090 [21].

$$m_{pres} = \frac{P_{pres_i} \cdot V_{pres_i}}{R \cdot T_{tank}} + 20\% \quad (3.8)$$

3.2.3 Tanks Sizing

Since the chosen feeding system is a Blowdown architecture, both propellant and pressurant are stored in the same tanks. In order to retrieve their parameters, a preliminary analysis is performed to estimate the available volume onboard the SVM. No official data can be found in the literature; therefore, by analyzing the external dimensions of the bus, a cylinder 1 m in height and 1.42 m in diameter is set as the maximum available space for the tanks.

The total tank volume required for the mission is retrieved using equation 3.9, where a 1% margin is added for internal components [21].

$$V_{tank} = (V_{pres_i} + V_{prop}) + 1\% \quad (3.9)$$

As the first iteration, a single spherical tank is considered. Although compliant with the dimensions requirements, having a single tank generates excessive pressure drops throughout the lifetime of the mission as a consequence of the chosen feeding strategy; for this reason, a two-tank design is considered. However, due to



geometry restriction, this solution is discarded and a switch to a cylindrical shape is performed.

The optimal solution is found in a four tanks architecture, allowing for better pressure distribution and increased redundancy of the system. The selected material is Aluminum, compatible with atmospheric reentry standards, while the thickness of the tank is computed using equation 3.10, with $\sigma = 503$ MPa

$$t_{cyl} = 2 \cdot \frac{P_{pres_i} \cdot r_{cyl}}{\sigma} \quad (3.10)$$

Results are reported in table 3.5.

3.2.4 Required Thrust Level Justification

To begin the estimation of the number of engines, the thrust level for a Routine Operation maneuver is needed. As reported in section 3.1.1, these maneuvers are preceded and followed by a slew operation to reorient the SC. These reorientations, which take approximately ten minutes each, must be performed in eclipse conditions as well, restricting the time window available to perform OOP and IP from almost thirtythree minutes to around ten. Therefore, the burning time is retrieved as $t_b = t_{eclipse} - 2 \cdot t_{slew}$ and the thrust is computed with equation 3.11.

$$T = m_{sc_{wet}} \cdot \frac{\Delta v}{t_b} \quad (3.11)$$

The graph below correlates the required thrust level to the number of burns.

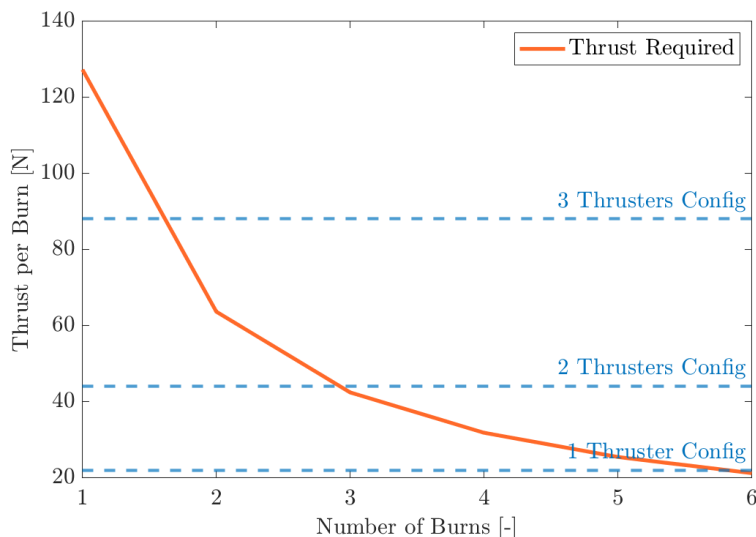


Figure 3.3: Thrust required per number of burns

To satisfy the constraint of having low-thrust engines compatible with ADCS maneuvering, a set of two 22.7 N thrusters is chosen [1]. Thus implying the need of three eclipses to perform each Routine Operation. This value is found to be one burn more with respect to the real scenario due to the statistical overestimation of the spacecraft's dry mass.

3.2.5 Results

The overall mass of the system is computed as follows, with $m_{thruster} = 0.70$ kg [8]:

$$m_{PS} = (16 \cdot m_{thruster} + 4 \cdot m_{tank} + m_{pres}) + 10\% \quad (3.12)$$

Table 3.5 summarizes the output of the sizing process.



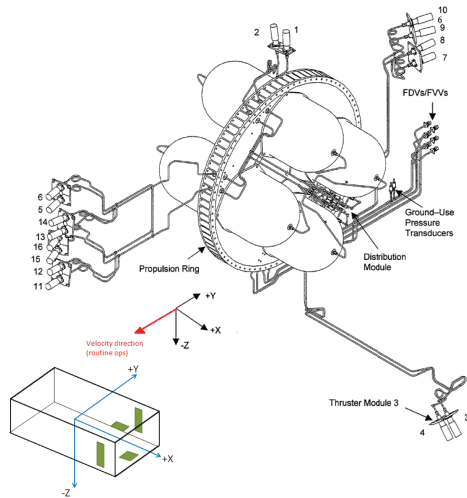
	Estimated	Real
Spacecraft Dry Mass [Kg]	4260	3769
Propellant mass [kg]	353	316
Propellant Tank Volume [L]	387	-
Initial Helium Pressure [Bar]	291	-
Final Helium Pressure [Bar]	65.5	-
Single Tank Mass [Kg]	40	-
Single Tank Thickness [cm]	1.25	-
Single Tank Radius [m]	0.216	-
Subsystem Mass Budget [Kg]	189	-

Table 3.5: Reverse Engineering Results

3.3 Outputs

3.3.1 Configuration

The Propulsion Subsystem is composed of four independent propellant tanks coupled in pairs for redundancy. Each tank feeds a set of eight thrusters, installed onto four separate propulsion plates - green area in figure 3.4. Their configuration is described in table 3.6



Thruster N°		Thruster Function	
Prime	Redundant	Torque	Thrust
1	2	+Y	-
3	4	-Y	-
5	6	-X	-
7	8	-Z	-Y
9	10	+Z	-Y
11	12	+X	-
13	14	+Z	+Y
15	16	-Z	+Y

Table 3.6: Thruster Module Configuration And Function [2]

Figure 3.4: PS configuration [2]

Out of the sixteen thrusters present onboard, only eight - four nominal and four redundant - are employed to give the maneuvering Δv , specifically:

- T7 and T9 are used for IP burns,
- T13 and T15 are used for OOP burns.

The remaining engines are used for ADCS purposes. A distribution module is placed between the tanks and the thrusters to guarantee cross-feeding capabilities; a set of valves is also present for fill, drain, and vent operations.



4 | Telemetry and Telecommunication Subsystem

Change Log	
Section	Content
4.1.2.3	Page [21] ; Added transmitted power, transmitter gain and line losses to quantify EIRP.
4.1.2.3	Page [21] Added system level noise temperature reference

Table 4.1: TTMTTC Change Log Table

4.1 TTM&TC Architecture

The Metop-A TTM&TC architecture is outlined in table 4.2 and in the electrical structure diagram 4.1. The physical positioning of the antennae can be seen on 4.2. All antennae are located in the same face.

The spacecraft is controlled by EUMETSAT from the Kiruna Ground Station. The system is equipped with two S-band omnidirectional antennas paired with a 3 dB hybrid coupler. Downlink is performed at 2230 MHz with 4.096 kbit/s in SP-L/PSK/PM. The chosen modulation ensures more reliable communication by decreasing the number of symbols per bit. Similarly, telecommand uplink is done at 2053.4 MHz in NRZ/ PSK/ PM at 2 kbit/s. The X-band antennas are used to transmit the global data dump at 70 Mbps in QPSK each orbit to be downlinked at the Svalbard Svalsat Ground Station. The data is encoded with Reed-Solomons 255,223 concatenated with a convolutional encoding rate of 1/2 [23]. The high frequency was selected for the high data volume generated over one orbit to be downlinked on one pass. This is necessary given the system has a Solid-State recorder with a capacity of 24 Gb at end-of-life, capable of storing the data generated during one orbit plus some additional margin. The same rationale is behind the modulation with QPSK transmitting more bits per symbol.

The High-Rate Picture Transmission (HRPT) L-band and Low-Rate Picture Transmission (LRPT) VHF antennas are constantly broadcasting data, which allows meteorological station to access data about their location in real time. The L-band allows regional meteorological agencies to receive data regarding their region in real-time while the LRPT VHF antenna allows for anyone with an inexpensive receiver to acquire data.

The system is also equipped with an advanced data collection system (A-DCS) that provides environmental data to the Argos system and a Search and Rescue (SARR) beacon.

Function	Frequency	Useful Bit Rate
TTM (downlink)	S - band, 2230 MHz	4.096 kbit/s in SP-L/PSK/PM
TC (uplink)	S-band, 2053.4 MHz	2 kbit/s in NRZ/PSK/PM
Global Data Stream downlink	X-band 7750-7900 MHz	70 Mbit/s in QPSK
LRPT downlink	VHF 137.1 MHz	72 kbit/s in QPSK
AHRPT downlink	L-band 1701.3 MHz	3.5 Mbit/s in QPSK
A-DCS data reception	401.65 MHz	
A-DCS data transmission	UHF 466 MHz	200 or 400 bp/s bi-phase PM
SARR beacon-signal reception	121.5, 243, and 406.05 MHz	
SARR transmission	1.544 GHz	

Table 4.2: TTM&TC properties

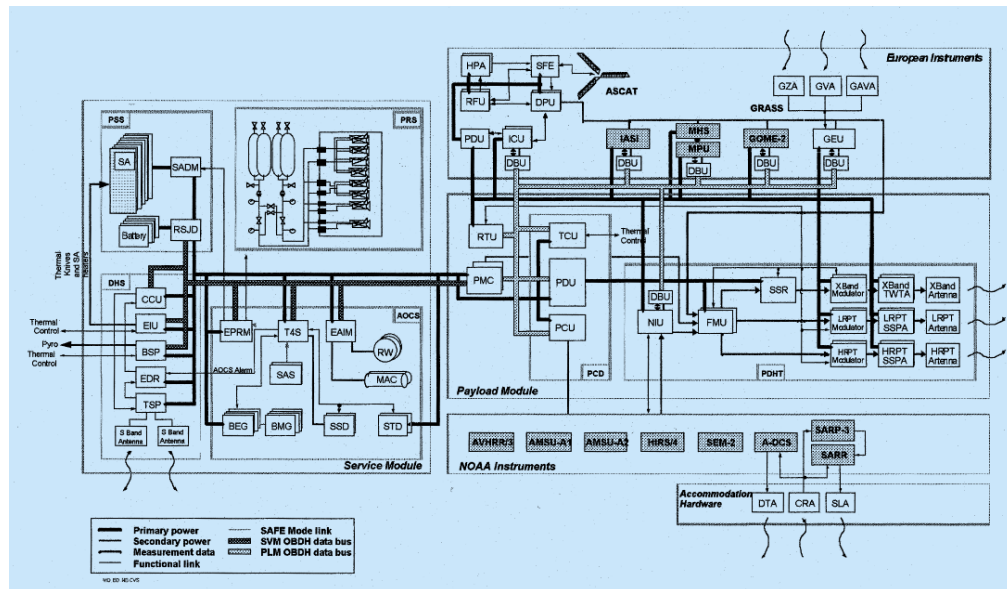


Figure 4.1: Metop's electrical architecture [3]

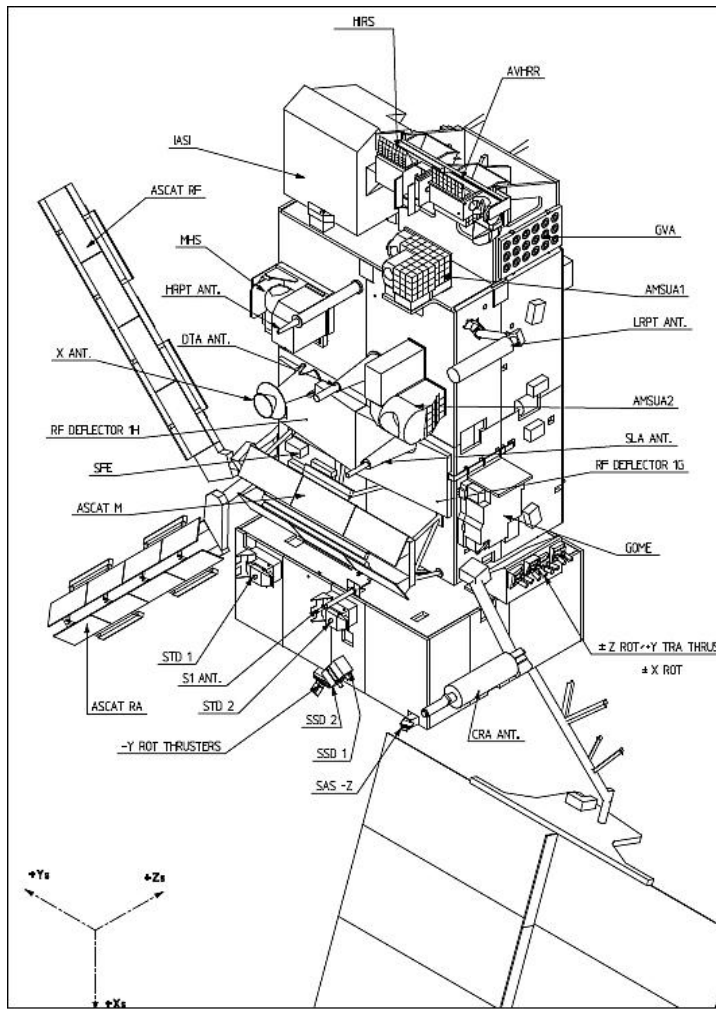


Figure 4.2: Metop spacecraft [1]

4.1.1 Data Volume Analysis

Data Volume is directly related with the available coverage with ground station. The preliminary design is performed assessing connectivity with SvalSat with the 70 Mbps, located at 78°13' N and 15°24' E. Due to the



high latitude, along with KSAT Troll Satellite Station in Antarctica, it is the only station capable of connecting with low altitude polar orbiting satellites on every revolution. GMAT is used to simulate the operational orbit of MetOp-A.

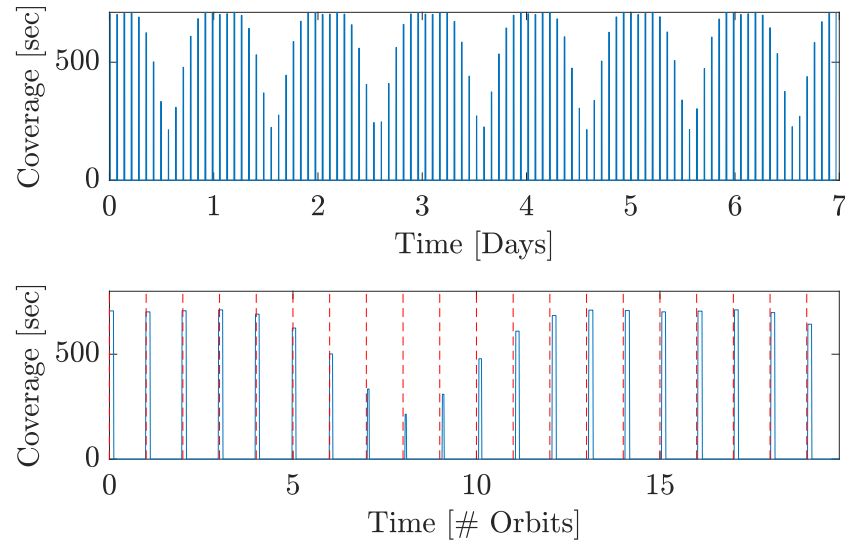


Figure 4.3: Metop's Coverage with SvalSat

As seen in the bottom graph of Figure 4.3, every orbit of MetOp-A has a coverage window. The minimum of which is around 215 seconds, with a maximum of 710 seconds. The periodicity of 1 day of this variation is observed on the top graph of Figure 4.3.

Similarly, S-band coverage with Kiruna Ground Station KIR-2 ($67^{\circ}52$ N and $20^{\circ}59$ E) [24] is assessed. The lower latitude of the station does not allow for visibility of MetOp-A on all orbits. As seen in Figure 4.4, 10 out of every 14 orbits have visibility, where 10 consecutive orbits attain connection followed by 4 blackout orbits. The comparison in visibility time is represented in Figure 4.4. Maximum coverage in an orbit is also 710 seconds.

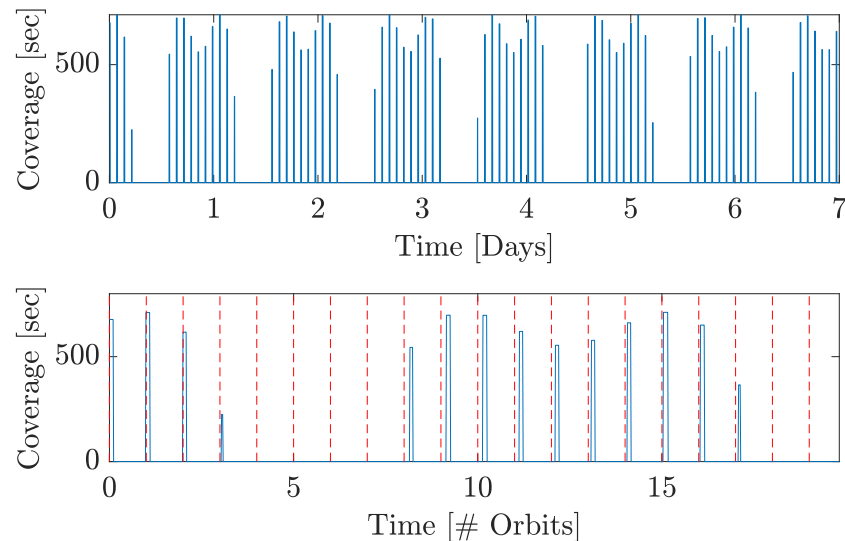
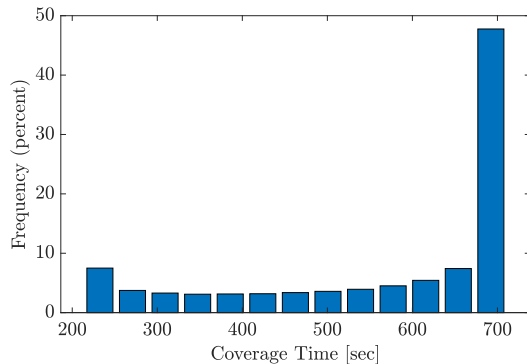


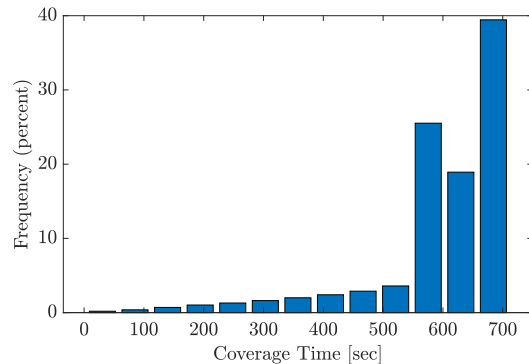
Figure 4.4: Metop's Coverage with Kiruna KAR-2



Distribution of the coverage time is seen in Figure 4.5. For SvalSat and the Global Data Dump, 50% the orbits have a coverage window of over 660 seconds or 11 minutes. Kiruna ground station also presents a 710 second maximum time window, however, due to consecutive black-out orbits, the maximum blackout time is 8 hours and 25 mins (30300 seconds).



(a) SvalSat



(b) Kiruna KAR-2

Figure 4.5: Coverage Time Window Histograms for SvalSat and Kiruna Ground Stations

Total Instrument Data Rate amounts to 3.47 Mbit/sec in Nominal Operational Mode. This yields a data volume of 21 Gbs, which is less than the maximum storage capacity of the solid state recorder of 24 Gbit [1]. With the 70 Mbit/sec X-band data rate with SvalSat station, a total of 343 seconds are needed to dump the theoretical maximum of 24 Gbits, and 300 seconds to downlink the nominal 21 Gbits. Looking at Figure 4.5a, 15.75% and 12.12% of the passages above SvalSat would not be able to down-link the theoretical maximum and Operational Data, respectively.

4.1.2 Link Budget

The link budget is calculated for the cases of data dump, telemetry downlink and tracking and telecommand uplink. LRPT and AHRPT were not considered in this analysis. The link budget is calculated using the equation:

$$\frac{E_b}{N_0} = P + L_l + G_t + L_s + L_a + G_r + L_p - 10\log_{10}k - 10\log_{10}T_s - 10\log_{10}R \quad (4.1)$$

The slant range is calculated for the worst case scenario, with an elevation of 10 degrees. It is calculated by solving the triangle with vertices in the center of the earth, the satellite's position and the ground station.

The free space losses are estimated using the equation:

$$L_s = \left(\frac{\lambda}{4\pi S} \right)^2 \quad (4.2)$$

Atmospheric losses are obtained from [23], Metop's Second Generation Report that features the same orbit. Pointing losses are assumed for worst case at 1 dB. The system noise is taken from Table 13-10 in SMAD[25]. The receiver gain is calculated using the following equation:

$$G_r = \frac{\pi^2 D_r^2 \eta}{\lambda^2} \quad (4.3)$$

The Svalsat and Kiruna antennas both have a diameter of 11 meters.[26][24] For the uplink case, given the lack of documentation regarding Metop A antenna, the S-band omnidirectional antenna by L3Harris was taken as reference [27]. The Signal-to-Noise ratio was calculated using

$$SNR = \frac{E_b}{N_0} + 10 * \log_{10}\left(\frac{R}{B}\right) \quad (4.4)$$

Bandwidths were retrieved from the Observing Systems Capability Analysis and Review Tool website [28]. The results are outlined in 4.3. In all cases the SNR is larger than 10 dB.



4.1.2.1 X - Band Global Data Dump Link

The data transfer link was calculated with the EIRP obtained from Metop-Second Generation link budget[23]. The equation simplifies to:

$$\frac{E_b}{N_0} = EIRP + L_s + L_a + G_r + L_p - 10\log_{10}k - 10\log_{10}T_s - 10\log_{10}R \quad (4.5)$$

The code rate and required budget are also taken from the SG report [23]. The budget of 8.55 dB for data transfer is in accordance with the one from the second generation of Metop at 7.7 dB, though the report considers some additional losses not included in this calculation. The margin is 5.47 dB, above the recommended value of 3 dB.

4.1.2.2 TM Downlink Budget and TTC Uplink Budget

The downlink budget is calculated using the transmitted power of 10 W from the selected antenna [27]. The code rate is taken as 1 by assuming the encoding and modulation coefficients to be equal. For the uplink budget the transmitted power was taken as the maximum available power in S-band for the Kiruna station at 200 W [29]. The receiver gain is obtained from the datasheet provided by Harris [27]. Considering a minimum of 10 dB, the margins are 12 and 19 dB for downlink and uplink respectively.

4.1.2.3 Results

Parameter (dB)	Global Data Stream	TM Downlink	TC Uplink
Transmitted Power (dBW) [23][27] [29]	19.93	10	23
Transmitter Gain (dBi) [23][27] [24]	6.50	1	45
Line losses (dB) [23][27] [30]	1.85	-	3
EIRP (dBW)	24.58	9.0	65.89
Free space Loss (dB)	193.87	183.00	182.28
Atmospheric Loss (dB)	2.88	2.88	2.88
Pointing Loss (dB)	1	1	1
Receiver Diameter (m)	11	11	-
Receiver efficiency	0.55	0.55	-
Receiver Gain (dB)	56.47	45	1
System Noise (dB K) [31]	21.3	21.3	27.9
Bit Rate (bit/s)	$70 * 10^6$	4096	2000
Code Rate	2.29	1	1
Link Budget (dB)	8.55	38.90	48.42
Required Eb/N0 (FER = 10^{-6}) (dB)	3.08	10	10
Link Margin (dB)	5.47	28.90	38.42
Bandwidth (kHz)	63000	1500	2000
SNR (dB)	13.27	12.01	19.67

Table 4.3: Link Budget



5 | Attitude Determination and Control Subsystem

5.1 System Analysis

5.1.1 Architecture

The attitude control architecture is based on three units, which perform the interface between the service module and the sensors and actuators. These units are:

- T4S: in charge of the interface between the Earth sensors, Sun sensors, gyros and the Solar Acquisition Sensor (SAS) [32] [3]
- EAIM: in charge of the monitoring and command for the reaction wheels and magnetotorquers [3]
- EPRM: in charge of the command and acquisition capability of the propulsion subsystem. This unit also provides the interface between the mentioned subsystem and the solar-array mechanism [3]

The sensors used in this subsystem are two digital Earth sensors for the roll and pitch axis, two digital Sun sensors for the yaw and four independent two-axis gyros. The digital sensors have one level of redundancy each, while the gyros have two. Given that each digital sensor gives information on the attitude of one different axis, it's very important to maintain at least one level of redundancy. On the other hand, since all of the modes use gyros for the attitude determination, especially the safe mode, it's important to have a higher level of redundancy.

Sensor	Quantity	Redundancy level
Digital Earth sensor	2	1
Digital Sun sensor	2	1
Gyro	4	2

Table 5.1: Sensor's redundancy

The use of an Earth sensor or a magnetometer for this specific mission would be appropriate since this spacecraft is Nadir pointing and in a low orbit. Nevertheless, as good pointing accuracy is needed, the first sensor is a better choice.

Annexing an additional sensor is necessary for the full attitude determination, a star sensor would allow to do the full attitude determination while also having the highest accuracy. This sensor was used on the first generation of MetOp satellites [33] but it was discarded for the following mission (MetOp-A), possibly because the higher precision was not necessary, and a simpler sensor could be used. Therefore, the best option to fulfil the attitude determination and maintain the high accuracy is the implementation of a Sun sensor. Finally, the presence of the gyros is needed since the Sun could lay out of the FOV of the Sun sensor, on the other hand this kind of sensor is useful for non-nominal modes.

The actuation for the attitude control is done through two magnetotorquers and three reaction wheels, none of which has redundancy. This choice is likely due to the high level of redundancy in the thrusters, if any of the mentioned actuators fails, the thrusters by themselves could guarantee full control of the spacecraft.

There are sixteen thrusters, meaning eight functioning thrusters plus one redundant (not active) thruster for each one. It's important to clarify that these actuators are the same used in the propulsion subsystem, its configuration can be seen in that section.

Actuator	Quantity	Redundancy level	Value
Reaction wheel	3	0	40 ms
Magnetotorquer	2	0	315 Am ²
Thruster	8	1	23.5 N

Table 5.2: Actuator's characteristics

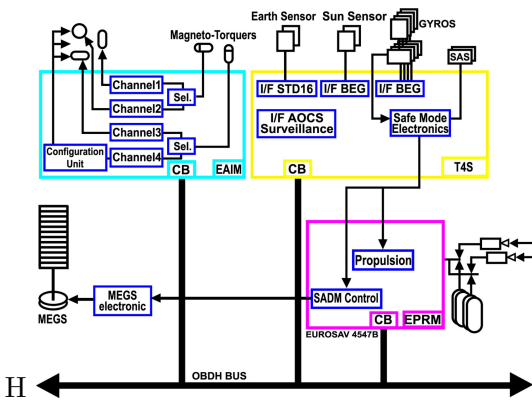


Figure 5.1: Architecture of the ADCS subsystem

The implementation of reaction wheels allows to have a better pointing accuracy for small angles. Since the spacecraft lays in a low orbit, the use of a set of magnetotorquers can give torque in two of the axes, therefore enabling the desaturation of the reaction wheels. As it will be explained in the following section the slew manoeuvre is performed by the thrusters, the addition of a control moment gyro would only lead to a heavier spacecraft with no advantages on the performance.

Finally, there is the Solar Array Drive Mechanism (SADM) which acts as an independent one-axis control for the solar panels, increasing its accuracy and allowing for good pointing during operations. As the power demand is quite high, and MetOp-A needs to be Nadir pointing during a great part of its lifetime, the implementation of this independent mechanism is justified.

In the figure 5.1 it is possible to appreciate the architecture of the attitude and orbit control subsystem. The different units are represented with different colours.

5.1.2 Control Modes

The MetOp-A control modes can be split into two main types. Nominal control modes are in charge of the daily and planned operation of the spacecraft. Non-nominal control modes are related to the safe mode and recovering the attitude to continue with nominal operations.

5.1.2.1 Nominal Control Modes

The nominal control modes are [33] [34]:

- Yaw Steering Mode (YSM). It is the primary AOCS operational mode of MetOp-A. It performs a Nadir pointing with all the instruments pointing towards Earth for data acquisition. Yaw steering sets the yaw angle so the solar arrays have maximal lighting without changing the roll and pitch.
- Fine Pointing Mode (FPM). It is a steady-state transition mode between some of the thruster's control modes and YSM. The change between reaction wheels and magnetotorquers to only thrusters is performed during this mode
- Orbit Control Mode (OCM). Is the mode applied to perform both In-Plane (IP) and Out-Of-Plane (OOP) manoeuvres with long thrust duration. In the case of OOP, the payload mission is interrupted, and a first 90 deg rotation is performed around Z-axis to point the thrusters properly. However, for the IP manoeuvres, the payload is kept active. This mode is divided into two sub-modes in table 5.3 to distinguish between IP and OOP
- Fine Control Mode (FCM). It is alternatively used for orbit IP corrections with small amplitude. It is identical to YSM and can only be accessed through that specific mode
- Solar Array Drive Mechanism (SADM). It is the independent one-axis control used to point the solar panel towards the Sun.



5.1.2.2 Non-Nominal Control Modes

The non-nominal control modes are [33] [34]:

- Safe Mode (SFM). Ensures survival state after a major anomaly. The satellite goes to Sun pointing and starts spinning at a restricted rate
- Rate Reduction Mode (RRM). It is used during initial acquisition after the solar array secondary deployment, in re-acquisition cases after failures, and returning to nominal operations from safe mode. It is intended to reduce the angular rates to a threshold value in the three axes, and while doing that, the spacecraft has an arbitrary attitude
- Coarse Acquisition Mode (CAM). Allows to obtain a specific accuracy in both roll and pitch angle and geocentric pointing while having a controlled rotation along the yaw axis
- Fine Acquisition Mode 1 (FAM1). Performs yaw acquisition while maintaining a geocentric pointing with the pitch and roll axes. There is an automatic transition to FAM2 if the accuracy and rates are lower than a specific threshold
- Fine Acquisition Mode 2 (FAM2). It is a stable waiting mode coinciding with the acquisition phase ending. It maintains satisfactory pointing performances while reducing the hydrazine consumption
- Fine Acquisition Mode 3 (FAM3). It is an intermediate mode between FAM2 and FPM. Its main objective is to set up the wheel velocity to an adequate initial value, such that the wheel kinetic momentum transient is reduced when entering OPM

5.2 Reverse Engineering

5.2.1 Pointing Budget

5.2.1.1 Pointing Requirements

The needs of every subsystem are analysed to determine the pointing requirements of the MetOp-A spacecraft.

Regarding PL, and using the specifications that were shown in the first Homework, the swath width or FoV of each payload is retrieved. The FoV of all the payloads are obtained using equation 5.1, where h is the altitude of the orbit and SW is the Swath Width.

$$FoV = \arctan \frac{SW}{2 \cdot h} \quad (5.1)$$

Beware that this is a very preliminary and rough approximation, therefore, the found values might be far from the real ones. According to these computations, the most demanding payload in terms of pointing requirements is ASCAT, whose value is 18.6 deg

From TTMT the main pointing requirement comes from the x-band isoflux antenna. The beamwidth is obtained from reference [35]. From there, to achieve a gain of +3 dB, a value of 50 deg of beamwidth is needed. The pointing requirement is set to be half of this value, therefore 25 deg

In the case of TCS, the main parts that need specific pointing are the radiators. As they are placed in the side face of the MetOp-A (which is not pointing towards Nadir) and are perpendicular to the solar panels, the pointing is passively achieved. Therefore no pointing requirement is needed.

The last pointing requirement comes from EPS. The value has been fixed to 30 degrees as it is considered the maximum admissible inclination with respect to sunlight to obtain satisfactory power [8].

5.2.1.2 Achieved Pointing

Both table 5.3 and 5.4 show in detail the control modes, actuators and sensors and the accuracy reached [33] [34]. In these tables, DES refers to Digital Earth, DSS to Digital Sun Sensor, RW to Reaction Wheels and MT to Magnetotorquers.



Mode	Sensors	Actuators	Accuracy [deg]
FPM	1 DES, 1 DSS and 2 gyros	8 thrusters	AKE < [0.07 (X) 0.10 (Y) 0.17 (Z)], APE < 1
YSM	1 DES, 1 DSS and 2 gyros	RW with MT	AKE < [0.07 (X) 0.10 (Y) 0.17 (Z)], APE < 1
OCM (OOP)	1 DES and 2 gyros	8 thrusters	AKE < 0.25, APE < 1
OCM (IP)	1 DES, 1 DSS and 2 gyros	8 thrusters	AKE < [0.07 (X) 0.10 (Y) 0.17 (Z)], APE < 1
FCM	1 DES, 1 DSS and 2 gyros	RW with MT	AKE < [0.07 (X) 0.10 (Y) 0.17 (Z)], APE < 1
SADM	-	KARMA-5 SG	AKE < [0.07 (X) 0.10 (Y) 0.17 (Z)], APE < 0.2

Table 5.3: Nominal modes description and accuracy

Mode	Sensors	Actuators	Accuracy [deg]
RRM	1 DES, 1 DSS and 2 gyros	8 thrusters	AKE < [0.07 (X) 0.10 (Y) 0.17 (Z)], APE < 1
SFM	2 SAS (+Z and -Z) and 2 gyros	8 thrusters	AKE < 1, APE < 1
CAM	1 DES, 1 DSS and 2 gyros	8 thrusters	AKE < [0.07 (X) 0.10 (Y) 0.17 (Z)], APE < 1
FAM1	1 DES and 2 gyros	8 thrusters	AKE < 0.25, APE < 1
FAM2	1 DES, 1 DSS and 2 gyros	8 thrusters	AKE < [0.07 (X) 0.10 (Y) 0.17 (Z)], APE < 1
FAM3	1 DES, 1 DSS and 2 gyros	8 thrusters	AKE < [0.07 (X) 0.10 (Y) 0.17 (Z)], APE < 1

Table 5.4: Non-Nominal modes description and accuracy

The first task is to define and analyse the Absolute Knowledge Error (AKE).

For nominal operations and all the control modes that use the same sensors, 1 digital Sun sensor, 1 digital Earth sensor and 2 gyros, the achieved AKE is 0.07 deg (X-axis), 0.10 deg (Y-axis), 0.17 deg (Z-axis) [1].

Instead, for the control modes that use only 1 digital Earth sensor and 2 gyros, the AKE will be bigger (more error). The worst-case scenario coming from class notes is used [8], in this case, 0.25 degrees, which increases the value obtained during nominal operations.

Then, only 2 SAS and 2 gyros are used during the safe mode. The SAS also known as coarse Sun sensor, is used to acquire the Sun position with respect to the sensor foresight. This sensor helps to point the solar panels during the safe mode, where all the other sensors are turned off except the gyroscopes. The accuracy of this type of sensor is less than 1 deg [36]. The AKE of the whole self mode is set to be that value.

Regarding the Absolute Pointing Error (APE) for the nominal operations of MetOp-A, an analysis based on general considerations is made. It is a satellite using Sun and horizon sensors, which also has magnetotorquers included for desaturation and reaction wheels as main actuators. The required accuracy can be set to be between 1 and 5 degrees [8]. To choose a value, it is found through literature that the MetOp SG, which also uses reaction wheels, has an APE of less than 4 mdeg [37]. Moreover, the APE during FAM1 control mode, which is one of the intermediate modes to recover nominal operations, is 2 deg [34]. Considering this information, the APE for the MetOp-A operational phase is set to the minimum value of the available range, therefore, 1 deg.

For the modes that use thrusters as main actuators, the APE can be set to be 1 degree as it is still a Reaction Control System (RCS) [8].

Regarding the solar panel, it has its own control called SADM. As explained before, it is a 1-axis controlled mechanism used along with the YSM to point the solar arrays with better accuracy. SADM, also called KARMA-5, has a pointing accuracy of 0.2 degrees [38]. Even though it's set to be at a constant value of 0.2 deg, it must be said that the accuracy of this control is linked to the control mode that is being used for the whole satellite as is used as an additional mode only for the solar panels.

Concerning the angular rates, during FAM1 the satellite must achieve an angular velocity of less than 0.05 deg/s in all the axes. On the other hand, the Rate Reduction Mode finishes when the angular rate is less than 0.3 deg/s [34]. These values represent strict requirements for non-nominal control modes. It can be explained by the fact that all the instruments on board must take measurements of the Earth, and high angular velocities can reduce the accuracy of these operations, a very critical point for an observational satellite.



5.2.2 Disturbances

Since the MetOp-A lays in a LEO, all the disturbances torque must be considered. For its calculation a simplified CAD model was made, to obtain the inertia matrix as well as the centre of mass. See figure 5.3

For the calculation of the disturbances, a worst-case scenario was considered, this means that the surfaces considered are the biggest ones, and the magnetic field is the highest found in the orbit (see figure 5.2).

For Solar Radiation Pressure (SRP) is considered as applied only on the solar panel, since it's the furthest surface from the centre of mass, and has a large area. It is calculated using equation 5.5.

On the other hand, for the calculation of the magnetic torque, as well as the sizing of the magnetotorquers, is considered the maximum and minimum values of the magnetic field, respectively, which are computed using the satellite's orbit, see figure 5.2. The residual dipole of the spacecraft is approximated to that of a class II non spinning satellite, therefore having a dipole moment per unit mass of $3.5 \cdot 10^{-3} A \cdot m^2/kg$ [39], with a total mass of 4613 kg (value calculated in the propulsion subsystem). The torque magnetic torque is calculated using equation 5.4.

The gravity gradient torque and drag, are calculated implementing equations 5.2 and 5.3 respectively. These cannot be considered negligible a priori, since the spacecraft is in a LEO. The values used for the radius of the orbit, velocity of the spacecraft and density, are taken from the mission analysis, while the $c_d = 2.2$ [8] and the maximum deviation of the axis is 5 deg.

In the table 5.5 are presented the values obtained for each torque, note that the only one that could be negligible is the drag. Beware that the total torque considered does not correspond to the sum of the single disturbances, since a 100% of margin was applied.

Type	Torque
Gravity gradient	$8.3 \cdot 10^{-3}$
Solar pressure radiation	$2.9 \cdot 10^{-3}$
Drag	$5.4 \cdot 10^{-4}$
Magnetic torque	$6.3 \cdot 10^{-3}$
Total (+100% of margin)	$2.47 \cdot 10^{-2}$

Table 5.5: Distrubance torques

The results presented, even though calculated with several simplifications, are similar to the ones found with more complex and realistic models [40].

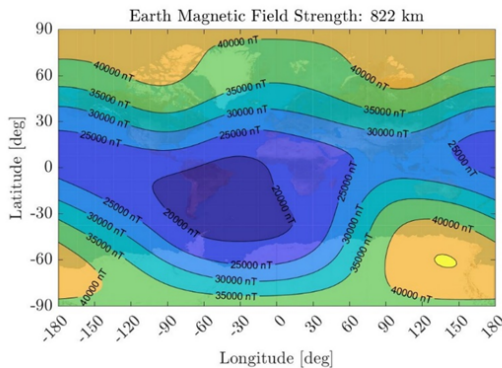


Figure 5.2: MetOp-A in orbit magnetic field

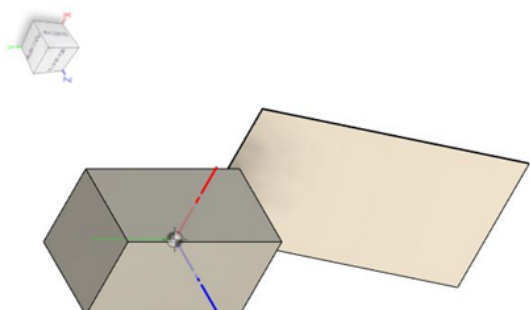


Figure 5.3: Simplified CAD model of MetOp-A

$$(5.2) \quad T_{gg} = \frac{3\mu}{2R_{orb}^3} (I_{max} - I_{min}) \sin 2\theta$$

$$T_{drag} = \frac{1}{2} \rho c_d A v^2 (c_{ap} - c_g) \quad (5.3)$$

$$(5.4) \quad T_{mag} = DB$$

$$T_{SRP} = \frac{F_s}{c} A_s (1 + q) (c_{sp} - c_g) \cos I \quad (5.5)$$



5.2.3 Slew Manoeuvres

The slew manoeuvre is calculated using the data presented in the architecture section, the slew angle is 90 deg as it is the requirement to perform the OOP, as explained in the description of the Orbit Control Mode (OCM).

As shown in the mission analysis subsystem, three change of plane manoeuvres needed to be performed during the mission, for each one two slew manoeuvres must take place, therefore having a total of six slew manoeuvres.

This amounts to a total of 19.4108 kg of propellant. Calculated using equations 5.6 and 5.7, and considering that the thrusters have the smallest possible arm.

$$(5.6) \quad t_{slew} = \sqrt{\frac{\theta_m Iv}{n_t F_t L_t}}$$

$$(5.7) \quad m_{slew} = n_{slew} \frac{2n_t F_t t_{b-slew}}{I_{sp} g_0}$$

5.2.4 Pointing And Desaturation

As shown in the precedent section, the three reaction wheels and the magnetotorquers are used for the nominal mode. By calculating the angular momentum of the wheels as $h = 40 \cdot 3$ Nms, and the angular momentum of the disturbances with equation 5.10, it is demonstrated that the reaction wheels are capable of counteracting the disturbances. Considering the disturbance torque constant along the entire orbit, the reaction wheels saturate after 0.8 orbits, given that the orbit's period is $6.063 \cdot 10^3$ s.

Using equation 5.9 is seen that the magnetotorquers alone are not able to counteract the disturbances, therefore they are used to desaturate the reaction wheels. Take into account that the magnetotorquers can give torque along two axes, and so are not able to de-saturate the reaction wheel along the third one, this should not be a problem since the disturbance torque in that axis should be one order of magnitude smaller [40].

A more accurate analysis was performed by Pessina S., Gomes Paulino N.M.G., De Juana J.M. and Righetti P., in which is seen that the magnetotorquers work at maximum torque along the entire orbit, and the reaction wheels never arrive to the saturation limit.

In non-nominal modes, and some nominal as well, the thrusters alone are used for station keeping. To calculate the amount of force and propellant that is required to counteract the disturbance torques, equations 5.12 and 5.13 are used. Considering a worst-case scenario, on which the thrusters have the minimum possible arm, it's found that a total amount of 0.0049 kg of propellant are needed per orbit. For this calculation is assumed that the thrust is provided by pulses of 8 Hz [1] during the entire orbit.

$$(5.8) \quad T_m = D_m B_{min}$$

$$(5.9) \quad h_m = 2T_m T_{orb}$$

$$(5.10) \quad h_{dist} = T_{dist} T_{orb}$$

$$(5.11) \quad n_{orb} = \frac{h_{RW}}{h_{dist}}$$

$$(5.12) \quad F_{t-SK} = \frac{T_{tot}}{n_t L_t}$$

$$(5.13) \quad m_{p-SK} = \frac{n_{pulse} t_{pulse} F_{t-dist}}{I_{sp} g_0}$$

5.3 Outputs

5.3.1 Budgets

A qualitative consideration on the data that must be handled by the subsystem can be done, by studying the usual sampling time of the sensors used [41]:

- Sun sensor: 1-5Hz
- Earth sensor: 1 Hz
- Gyro: 40-1000 Hz

Note that the three sensors have very different sampling times, therefore it's important to allocate proper hardware and software to handle correctly the big difference in sampling rates.

On table 5.6 are shown the mass and power budget for the actuators and sensors of the ADCS subsystem.



Item	Mass [Kg]	Power [W]
Digital Sun sensor	2 [42]	3
Digital Earth sensor	3.5	200
Gyro	15	5
Reaction wheel	8.75 [43]	169 [43]
Magnetotorquer	7.8 [44]	11.4 [44]
Thruster (propellant)	20.38	-
Total	57.43	388.4

Table 5.6: Mass and power budget for the ADCS subsystem

5.3.2 Pointing Budget

Subsystem	APE per phase [deg]					
	LEOP		SIOV		Nominal	
	Required	Achieved	Required	Achieved	Required	Achieved
PL	-	1	18.6	1	18.6	1
TTMTC	-	1	25	1	25	1
TCS	-	1	-	1	-	1
EPS	30	0.2	30	0.2	30	0.2

Table 5.7: Satellite phases pointing budget (APE)

Table 5.7 shows the different APE required and achieved for the three main MetOp-A phases: Launch and Early Operations Phase (LEOP), Satellite In-Orbit Verification (SIOV) and nominal operations. All the TCS requirements are set to null since it is achieved passively, as previously explained. Nevertheless, the achieved pointing is the one obtained through the satellite's control mode.

During LEOP, all the instruments are switched off, so no pointing requirement is set. Besides, it is assumed that the omnidirectional antenna is used for the TTMTC. During this phase, the satellite must perform the detumbling where the angular velocities are high, and the isoflux antenna cannot be appropriately pointed. Nevertheless, it is important to start generating power so the EPS requirement comes from the solar panels. During LEOP the MetOp-A goes through several control modes until achieving the nominal YSM.

Both SIOV and nominal operations can be considered the same in terms of required accuracy. Since SIOV is like nominal operations but validations are performed, can be considered that they share the required APE. It is assumed that both use YSM, and the APE values are retrieved by this control mode (refer to table 5.3).

Finally, it is important to notice that the required and achieved APE values are quite different in all the phases and subsystems, meaning that the preliminary approach used to obtain the pointing requirements is very rough. In reality, the pointing requirements should be higher to match the achievable values, if not, the sensors and actuators would be oversized during the design phase. It must be said that pointing drift and rates have not been considered as no such information can be found for all the control modes and phases. Could be that these requirements are more restricted than the APE, as the instruments must have a stable pointing to obtain good measurements. With this global picture, it can be seen that a preliminary study and sizing, like the one performed during this project, is not enough to set accurately the pointing budget, but it is enough to have a first idea of the orders of magnitude and needs coming from the mission.



6 | Thermal Control Subsystem

Change Log	
Section	Content
6.2	Page [30]; Maximum and Minimum temperature update
6.2.1.1	Page [32]; Results update and radiator area justification
6.2.1.2	Page [32]; Results and equation 6.14 update
6.2.3	Page [33]; Internal nodes heat exchange addition
6.3.1	Page [34]; Outputs update

Table 6.1: TCS Change Log table

6.1 System Analysis

The Thermal Control Subsystem aims to maintain the spacecraft inside its allowable temperature ranges. Given the complexity of MetOp-A and its size, the following considerations are made:

- out of the eleven payloads hosted onboard, only three have a thermal interface with the PLM. The other eight are thermally decoupled from the spacecraft and have their own TCS. Therefore only AVHRR, HIRSS, and S&RSAT are considered for the design of this subsystem;
- given the elevated external surface of the spacecraft, high heat exchange with the environment is expected; therefore the optical properties of the outside coating shall be tuned accordingly;
- given the relevant size of the solar panel, a separate thermal analysis shall be performed to better characterize its behavior.

6.1.1 Thermal Environment

The satellite has internal and external heat sources. The external ones are the Sun, the Earth's albedo and the infrared radiation coming from the Earth. The internal power comes from the payload and the service modules, plus the three instruments that are thermally coupled with the system. Moreover, the deep space at 0 K is used to compute the thermal equilibrium with the radiator in Subsection 6.2.1.1.

The thermal control strategy differs for every mode and phase of the mission based on the environmental condition. Table 6.2 summarizes the different thermal situations to identify the worst hot case and worst cold case to then perform a preliminary sizing of the TCS.

LEOP			Operational Mode	
	Sunlit	Shadow	Science Mode	Eclipse
Q_{sun} [W]	x	-	x	-
Q_{alb} [W]	x	-	x	-
Q_{IR} [W]	x	x	x	x
Q_{SVM} [W]	x	x	x	x
Q_{PLM} [W]	x	x	x	x
Q_{AVHRR} [W]	-	-	x	x
Q_{HIRSS} [W]	-	-	x	x
$Q_{S\&RSAT}$ [W]	-	-	x	x

Table 6.2: Heat power in different phases

Since the orbit is circular, the external fluxes don't undergo a variation due to the altitude; however they vary because of other factors.



6.1.1.1 Worst Hot Case

Based on Table 6.2, the scientific mode is identified as the worst hot case. In this phase all the instruments are turned on at the same time and all the external fluxes are entering the system. To further stress the thermal condition, the environmental heat powers are maximized by assuming:

- the Earth's albedo at its maximum value of 0.39;
- the albedo factor equal to 1.

6.1.1.2 Worst Cold Case

In LEOP, the instruments are yet to be powered on, therefore, the worst cold case is identified in this phase. Moreover, during eclipses the only environmental power comes from the infrared radiation coming from the Earth. Hence, eclipse during the LEOP is identified as the worst cold case.

6.2 Reverse Engineering Study

To perform a preliminary sizing of the Thermal Control Subsystem, a mono nodal analysis is performed. Due to the geometry and configuration of the SC, the study is divided into:

- spherical mono nodal analysis on the main body of the SC;
- flat plate mono nodal analysis on the solar panel.

The materials considered for the analysis are: MLI for the exterior part of the spacecraft, Silvered FEP Teflon Tape for the radiator, white paint for the shadowed side of the solar panel and solar cells for the sunlit side. The optical properties of these materials are listed in Table 6.3.

Material	α	ϵ
MLI	0.2	0.03
Silvered FEP Teflon Tape	0.09	0.88
White Paint	0.18	0.88
Solar Cells	0.9	0.1

Table 6.3: Materials optical properties [7]

Table 6.4 compiles the operating temperature ranges of the components that are used to identify the allowed operating temperatures. Since the ranges of the batteries and of the hydrazine tanks are too stringent and the addition of the margin would result in the inversion of minimum and maximum temperatures, they are discarded from the mono nodal analysis. Therefore the reaction wheels' range is used as the baseline for the main body.

The minimum and maximum operating temperatures are defined as:

- $T_{MIN} = T_{MIN_{RW}} + 15 K = 278.15 K$ and $T_{MAX} = T_{MAX_{RW}} - 15 K = 298.15 K$, for the SC;
- $T_{MIN} = T_{MIN_{PAN}} + 15 K = 138.15 K$ and $T_{MAX} = T_{MAX_{PAN}} - 15 K = 368.18 K$, for the solar panel.



Component	T _{MIN} [deg]	T _{MAX} [deg]
OBDH	-20	50
Reaction Wheels	-10	40
Sensors	-30	50
Hydrazine Tanks	15	40
Batteries	0	15
Solar Panels	-150	110
Antenna	-100	100

Table 6.4: Components operating temperature ranges in degrees Celsius [8]

Component	Q _{intMIN} [W]	Q _{intMAX} [W]
Service Module	491	
Payload Module	437	
AVHRR	0	27
HIRS	0	24
SARR	0	86
Total	928	1065

Table 6.5: Installed onboard power [1]

Since eight out of eleven payloads are thermally decoupled from the system, the components considered to compute the maximum and minimum internally generated power are listed in Table 6.5, where:

$$F = \frac{1}{2} \left(1 - \frac{\sqrt{\left(\frac{h}{R_{Earth}}\right)^2 + 2\frac{h}{R_{Earth}}}}{1 + \frac{h}{R_{Earth}}} \right) \quad (6.1)$$

Additional data needed for the reverse engineering study are reported in Table 6.6.

a [-]	K _{diff} [-]	F [-]	T _{Earth} [K]	A [m ²]	A _{cross} [m ²]	A _{pan} [m ²]
Earth Albedo	Albedo Factor	View Factor	Earth Temperature	SC Area	SC Cross Area	Pannel Area

Table 6.6: Additional data

6.2.1 Spacecraft

To begin the analysis on the main body of the SC, the Sun, albedo, and infrared fluxes are computed as follows.

$$q_{sun} = q_0 = 1419 \text{ W/m}^2 \quad (6.2)$$

$$q_{alb} = q_0 \cdot a = 553.41 \text{ W/m}^2 \quad (6.3)$$

$$q_{IR} = \sigma \cdot \epsilon_E \cdot T_{earth}^4 = 370.58 \text{ W/m}^2 \quad (6.4)$$

The heat powers on the satellite due to the external fluxes are:

$$Q_{sun} = q_{sun} \cdot A_{cross} \cdot \alpha_{MLI} = 7622.86 \text{ W} \quad (6.5)$$

$$Q_{alb_{max}} = q_{alb} \cdot A \cdot F \cdot \alpha_{MLI} \cdot k_{diff} = 3192.7 \text{ W} \quad (6.6)$$

$$Q_{IR} = A \cdot F \cdot q_{IR} \cdot \epsilon_{MLI} = 320.68 \text{ W} \quad (6.7)$$

All of the maximum powers are summed to compute the worst hot case temperature 6.10 reached without any control. While for the worst cold case, only the infrared power and minimum internal power are considered.

$$Q_{sum_{HOT}} = Q_{sun} + Q_{alb_{max}} + Q_{IR} + Q_{int_{max}} = 12201 \text{ W} \quad (6.8)$$

$$Q_{sum_{COLD}} = Q_{IR} + Q_{int_{MIN}} = 1248.7 \text{ W} \quad (6.9)$$

$$T_{SC_{HOT}} = \left(\frac{Q_{sum_{HOT}}}{\sigma \epsilon_{MLI} A} \right)^{1/4} = 508.32 \text{ K} \quad (6.10)$$

$T_{SC_{HOT}}$ is outside the allowed temperature range; therefore, a passive control option must be analyzed.



6.2.1.1 Passive Control Sizing

To reduce the maximum temperature reached by the SC, a passive control solution through the use of a radiator is considered. The minimum area of the radiator needed to respect the temperature constraint is computed as follows:

$$A_{rad} = \frac{Q_{sum_{HOT}} - \sigma \varepsilon_{MLI} A T_{SC_{MAX}}^4}{\sigma \varepsilon_{rad} T_{SC_{MAX}}^4 - \sigma \varepsilon_{MLI} T_{SC_{MAX}}^4} = 21.15 \text{ m}^2 \quad (6.11)$$

A_{rad} is computed by assuming the temperature of the deep space - with which the SC performs a heat exchange - at 0 K.

As shown in 6.12, the computed A_{rad} allows enough power dissipation to bring down the maximum temperature within the limit. The computed value is found to be higher than expected; this is a downside of performing a mono nodal analysis where all units are condensed into a single point, and no specific thermal routing is defined. A more detailed analysis will lead to a reduction of this value.

$$T_{SC_{HOT}} = \left(\frac{Q_{sum_{HOT}}}{\sigma \varepsilon_{MLI}(A - A_{rad}) + \sigma \varepsilon_{rad} A_{rad}} \right)^{1/4} = 363.67 \text{ K} \quad (6.12)$$

6.2.1.2 Active Control Sizing

Finally, the worst cold case temperature can be computed by taking into account the presence of the radiator.

$$T_{SC_{COLD}} = \left(\frac{Q_{sum_{COLD}}}{\sigma \varepsilon_{MLI}(A - A_{rad}) + \sigma \varepsilon_{rad} A_{rad}} \right)^{1/4} = 179.53 \text{ K} \quad (6.13)$$

As expected, $T_{SC_{COLD}}$ is below the minimum allowed value. Therefore, an active control solution in the form of a heater is analyzed. The power provided by the heater 6.14 grants that the minimum temperature 6.15 stands within the optimal range. This power is derived by considering the radiator coupled to the rest of the system.

$$Q_{heater} = \sigma (\varepsilon_{MLI} (A - A_{rad}) + \epsilon_{rad} A_{rad}) T_{SC_{MIN}}^4 - Q_{sum_{COLD}} = 5945.5 \text{ W} \quad (6.14)$$

$$T_{sc_{COLD}} = \left(\frac{Q_{sum_{COLD}} + Q_{heater}}{\sigma \varepsilon_{MLI}(A - A_{rad}) + \sigma \epsilon_{rad} A_{rad}} \right)^{1/4} = 278.15 \text{ K} \quad (6.15)$$

The required heaters' power is well beyond the system's capabilities, representing almost double the entire available electrical power. This result is justified by the type of analysis performed since all the internal units' position is not modeled. To solve this issue, a multi nodal analysis with all the components is required, allowing the creation of thermal routes - for example, via straps - to better redistribute the internal heat and reduce the required power.

6.2.2 Solar Panel

The mono nodal analysis of the solar panel follows the same flow as the spacecraft's one. However, in this case, the heat power formulas for the flat plate analysis are used.

The heat powers are computed as:

$$Q_{sun_{pan}} = q_{sun} \cdot A_{pan} \cdot \alpha_{top} = 71965 \text{ W} \quad (6.16)$$

$$Q_{alb_{pan}} = q_{alb} \cdot A_{pan} \cdot \alpha_{top} \cdot k_{diff} \cdot \frac{R_{Earth}^2}{SMA} = 22049 \text{ W} \quad (6.17)$$

$$Q_{IR_{pan}} = A \cdot q_{IR} \cdot \epsilon_{bottom} \cdot \frac{R_{Earth}^2}{SMA} = 14436 \text{ W} \quad (6.18)$$

$$Q_{sum_{HOT}} = Q_{sun_{pan}} + Q_{alb_{pan}} + Q_{IR_{pan}} + Q_{int_{pan MAX}} = 112340 \text{ W} \quad (6.19)$$

$$Q_{sum_{COLD}} = Q_{IR_{pan}} + Q_{int_{pan MIN}} = 14436 \text{ W} \quad (6.20)$$



Since the allowed temperature range for the solar panel is broad, the worst cold case and worst hot case temperatures stand within said range without the need for thermal control solutions, as can be seen in 6.21 and 6.22.

$$T_{pan_{HOT}} = \frac{Q_{sum_{HOT}} - \eta_{pan} \cdot Q_{sun_{pan}}}{\sigma \cdot \left(\frac{1}{2}\epsilon_{top} + \frac{1}{2}\epsilon_{bottom} \right) \cdot 2A_{pan}}^{\frac{1}{4}} = 363.67 \text{ K} \quad (6.21)$$

$$T_{pan_{COLD}} = \frac{Q_{sum_{COLD}}}{\sigma \cdot \left(\frac{1}{2}\epsilon_{top} + \frac{1}{2}\epsilon_{bottom} \right) \cdot 2A_{pan}}^{\frac{1}{4}} = 260.58 \text{ K} \quad (6.22)$$

6.2.3 Multi Nodal Analysis

The results obtained in the previous section rely on the assumption that the entire spacecraft is modeled as a uniform sphere, no distinction is given between modules or subsystems. To further refine the TCS model, a multi-nodal analysis is implemented via the Simscape Software. The following nodes are taken into consideration:

- service module;
- payload module;
- solar panel;
- Hydrazine tanks.

Node	T _{MIN} [deg]	T _{MAX} [deg]
Service Module	15	55
Payload Module	-5	65
Solar Panel	-150	110
Hydrazine Tanks	15	40

Table 6.7: Nodes temperature ranges

All of them are considered thermally decoupled from one another, with the exception of Hydrazine Tanks and the SVM, as per MetOp-A design [1]. **The two of them exchange heat via radiation; black paint is used for the internal of the SVM while the tanks are covered in MLI.**

In this case, the PLM has a wider operating range, given by the OBDH, since the tanks are located in the SVM. The sizing is performed by iterating the radiator's area and heaters' power in order to ensure that each node stays in its operating temperature ranges - reported in table 6.7. The results are reported in Table 6.8 and Figure 6.1, as can be seen, all the nodes are in the correct operating ranges. Moreover, no need of heaters is required for the Solar Panel while the heaters budget for the tanks is already included inside the SVM one.

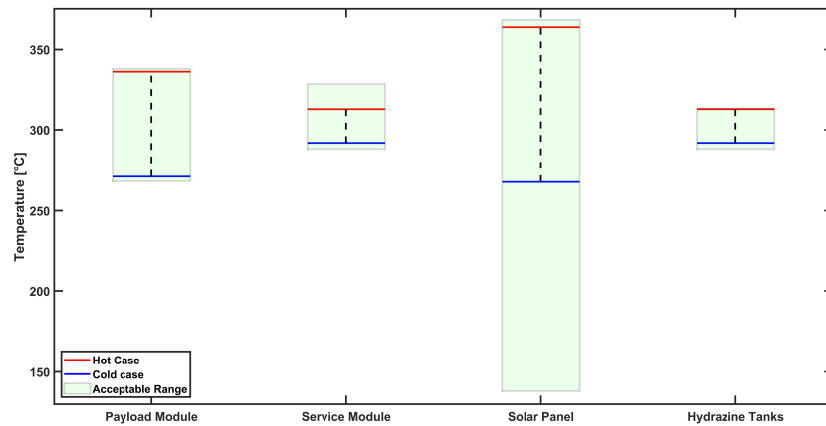


Figure 6.1: Temperature ranges of considered nodes

As already discussed during the mono nodal analysis, even in this preliminary multi nodal, the lack of knowledge of the internal disposition of the elements has the effect of producing an overestimation of the power of the required heater, which is well beyond the system's capability.



6.3 Outputs

6.3.1 Results

Table 6.8 summarizes the output of both sizing processes, mono nodal and multi nodal.

	Mono-Nodal		Multi-Nodal			
	SC	PAN	SVM	PLM	PAN	TANKS
$A_{rad} [m^2]$	21.15	-	5.9	12.7	-	-
$T_{HOT} [K]$	363.67	363.67	310.72	335.78	363.66	312.72
$Q_{heater} [W]$	5945.5	-	1800	3150	-	-
$T_{COLD} [K]$	278.15	260.58	291.92	271.00	267.68	291.92

Table 6.8: Reverse engineering results

6.3.2 Strategy & Configuration

MetOp-A Thermal Control System is based on a passive control strategy, with the supplement of heaters. All the units are internally mounted on aluminum honeycomb plates, with the internal sides covered with black paint to promote radiation heat exchange [45].

The external surface is instead covered by MLI made of ten layers with PLM and SVM radiators located mainly in the flight and anti-flight direction and zenith direction [46].

Instruments operating in the infrared spectrum require low working temperatures; therefore, they are located in a specific area called "balcony" - -x anti-Sun direction - which allows for a better view of deep space [46].

Two internal units require specific attention:

- **Batteries:** located inside a thermally isolated box and installed directly on a radiative surface [45];
- **Hydrazine tanks and lines:** entirely covered by MLI and with a set of dedicated heaters given their more strict temperature operating ranges.

Lastly, two types of heaters are installed onboard:

- **Operational Heaters:** controlled by the OBDH via thermistors and providing heat in all nominal operational phases [45];
- **Survival Heaters:** directly controlled by thermostats and granting thermal control in non-operational scenarios [45].

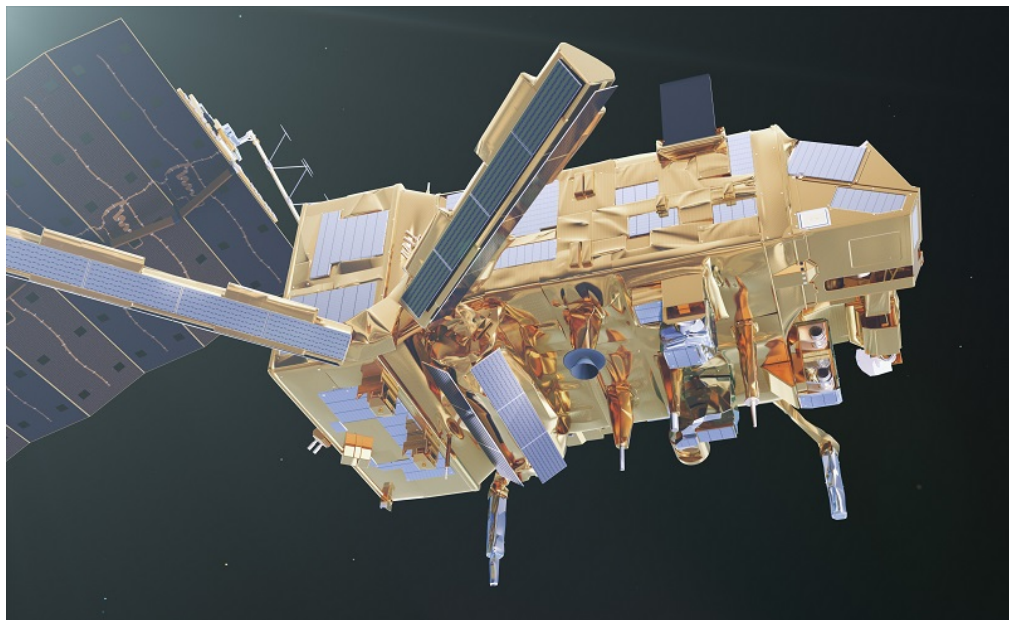


Figure 6.2: MetOp-A Artistic Representation

6.3.3 Budgets

The designed TCS has three major impacts on MetOp-A spacecraft subsystems:

- **EPS:** a power budget of 6005.50 W is required to make the heaters work;
- **OBDH:** a dedicated control unit and data budget is required on the OBDH architecture to monitor the temperature of the different nodes onboard the SC and command the heaters;
- **Structure:** a mass budget of 85.2 kg is retrieved considering the TCS as 2% of the estimated spacecraft dry mass [22].



7 | Electrical and Power Subsystem

7.1 System Architecture

Metop-A's architecture is outlined in Figure 7.1.

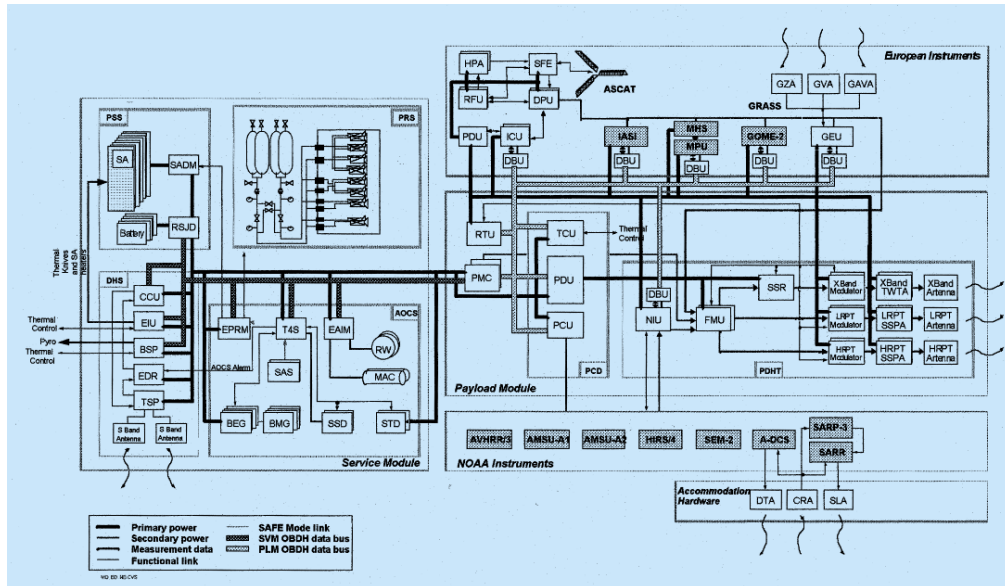


Figure 7.1: Metop-A's Electrical Architecture

7.1.1 Power Source

The primary power source consists of 8 Back Surface Reflector (BSR) solar panels, each of dimensions 1 x 5 m canted at 20 degrees weighing a total of 255 kg[1]. The solar arrays are heritage from the ENVISAT missions[47]. The Solar Array Drive Mechanism (SADM) rotates the panels to fix its orientation with respect to the sun.

7.1.2 Reverse Engineering Sizing

The solar array sizing is performed following the procedure used by Wertz [25]. Eclipse times are calculated using GMAT. The sizing is done for the worst case scenario yielding a time in eclipse of 1950 seconds and a time in daylight of 4133 seconds. The average power consumption over one orbit is 1813 W [1]. Because the power of the SVM is regulated through a shunt [47], the assumed distribution efficiencies are the ones of a DET system at 0.85 for daylight and 0.65 for eclipse [25]. The power that needs to be supplied by the solar array is calculated as:

$$P_{SA} = \frac{P_e T_e}{X_e T_d} + \frac{P_d}{X_d} = 3480W \quad (7.1)$$

Then, the EOL Power is calculated. The solar panel efficiency is set at 0.17, the efficiency of silicon based solar cells in the late 90s [48], when the mission was designed. The inherent degradation is set at the SMAD recommendation of 0.72 and multiplied by a coefficient of 0.8 for shadowing of cells, due to the 20 degrees cant angle of the panels [25]. The lifetime degradation at 2.75% per year, typical for these kind of cells [25]. The mission lifetime is 5 years [1] and theta is 23.34 degrees, coming from the 1-2 degrees incidence provided by SADM and considering the 20 degree cant angle [49]. The incident power from the sun is 1366 W/m². The EOL Power is then

$$P_{EOL} = P_i * \eta_{solar panels} * I_{degradation} * \cos(\theta_{incidence}) * (1 - L_{degradation})^{T_{life}} = 100.5533W/m^2 \quad (7.2)$$

Finally, the solar array area is calculated at:

$$A_{SA} = P_{SA}/P_{EOL} = 35.1m^2 \quad (7.3)$$



This is slightly smaller than the 40 m^2 present on the satellite. The reasons behind this might be several. First, the number calculated by the engineers might also be between 35 and 40. Given the use of 1x5 panels from heritage, the area might have been rounded up to the next multiple of 5. Second, the use of DET efficiencies is only an initial approximation. Given the complex electrical architecture of the system, the actual distribution efficiencies along the several lines and buses are most certainly lower. EO Portal lists the power supplied by the solar array at 2210 W at EOL, while the panels generate 3828 W EOL [47]. Therefore, the overall average transmission efficiency is 0.56.

7.1.3 Energy Storage

Energy storage consists of 5 Batteries of 40 Ah each, heritage from the SPOT missions. Data is given at beginning of life. To calculate the energy stored, the mean battery voltage is taken at 29V, the same one of SPOT-5 [50]. Total energy stored then becomes:

$$E = 5 * 40\text{ Ah} * 3600 \frac{\text{s}}{\text{h}} * 29\text{ V} = 208.8\text{ MJ} \quad (7.4)$$

Each battery weighs 47.4 kg, for a total weight of 237 kg. The specific energy is 28 Wh/kg and the energy density is 42 Wh/l [50]. Reverse sizing of the batteries is calculated using the same data from the solar array. From the equation, we can estimate the limit Depth of Discharge (DOD) used for the sizing.

$$C = \frac{P_e T_e}{(DOD) N \eta} \quad (7.5)$$

This yields a DOD of 25%. Considering the specific energy and energy density are on the lower end of the spectrum, and the calculated DOD, the batteries are assumed to be Ni-Cd[50]. This is confirmed by "Evaluation of Maximum Safe Voltage for Nickel-Cadmium Cells" [51].

7.1.4 Power Distribution Regulation & Control

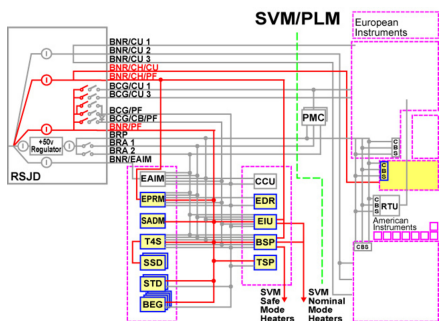


Figure 7.2: Main bus: Unregulated 22-39 V

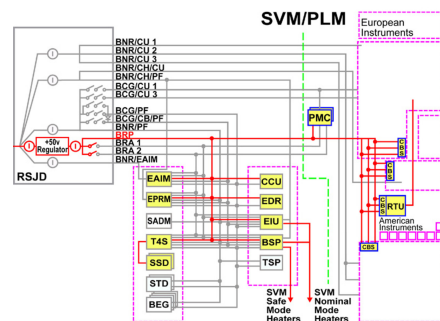


Figure 7.3: Permanent 50 V bus

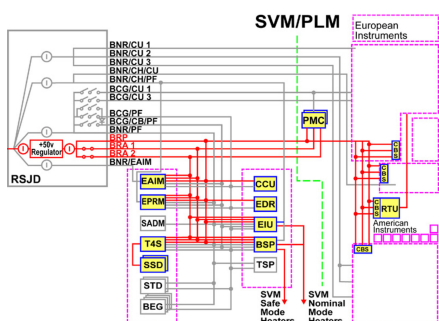


Figure 7.4: Switched 50 V bus

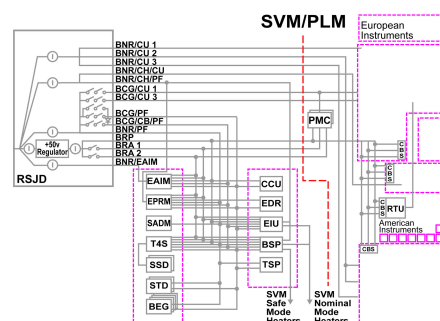


Figure 7.5: RSJD distribution



Power from the solar array and the batteries goes through the RSJD (Distribution and Shunt Junction Regulator). This system supplies power to the buses, controls the power demand and recharge of batteries, manages thermal control of the batteries, and is in charge of switching off lines in case of failures 7.5.

There are three buses present in Metop-A. The main bus is an unregulated 22-39 V bus which supplies the SVM in nominal and safe modes, the PLM avionics and thermal control, and the European instruments thermal control. A permanent regulated 50 V bus supplies the SVM low-level electronic functions and bus couplers, the Payload Module Controller (PMC) and EAIM and SVM thermal control heaters. A switched regulated 50 V bus, with the function of switching SVM and PMC bus couplers. The RSJD also supplies power to the Power Distribution Unit (PDU), which draws from the SVM to supply 22 – 37.5 V unregulated power to the PLM equipment and the European instruments, and to the Power Control Unit (PCU) which provides regulated power at 28 V to the US instruments. The Thermal Control Unit (TCU) supplies unregulated power to the heater mats.

The rationale behind the several buses and distribution units to ensure the integration of the several heritage and foreign platforms used in the satellite. The SVM is heritage from the SPOT missions designed for the unregulated voltage, the PLM is heritage from ENVISAT, and the US NOAA instruments are designed for a regulated voltage.

Instrument	Power [W]	Voltage [V]	Voltage Supply
A-DCS	72	28	Regulated
AMSU-A	99	28	Regulated
ASCAT	215	22-39	Unregulated
AVHRR/3	27	28	Regulated
GOME-2	42	22-39	Unregulated
GRAS	30	22-39	Unregulated
HIRS/4	24	28	Regulated
IASI	210	22-39	Unregulated
MHS	93	22-39	Unregulated
S&RSA	86	28	Regulated
SEM-2	10	28	Regulated
Total		908 Watts	

Table 7.1: Instrument Power Budget

7.2 Budget

Mass: Total mass is calculated as the mass of the panels, batteries and a 25% for cable and harnesses [52]. The upper limit for the margin is selected due to the large number of buses, harnesses and units. The total mass budget for the EPS is 656 kg. The power budget per subsystem and mission is described in Figure 7.6, all values are given in Watts.

It must be noted that the power seen in the different composition of the Service Module case does not represent the average consumption, but the ceiling value. For example, the Propulsion System may use up to 140 Watts during manoeuvring when firing 4 thrusters at the same time, with each valve consuming up to 30 Watts, with an extra for the Hydrazine Catalyst Thermal Control [18]. The ASCAT and GRAS system require an independent antenna deployment and functioning. This step is performed during LEOP to avoid problems later on [53]. Peak Instrument Power demand will take place during Global Data Dump, when the X and S band antennas are transmitting. Furthermore, the elevated value for ADCS during phases that require large attitude changes represents the peak demand based on the sum of the maximum power input for the reaction wheels and magnetometers.



Subsystem	LEOP			SIOV				Science Day	Science Eclipse	Manoeuvre	Transmission (X and S)	Disposal	Off-Nominal	Safe Mode
	Phase 1	Phase 2	Phase 3	Phase 1	Phase 2	Phase 3	Phase 4							
Instruments	0	110	110	110	110	110	908	908	589	110	908	0	110	0
A-DCS	0	0	0	0	0	0	72	72	72	0	72	0	0	0
AMSU-A	0	0	0	0	0	0	99	99	0	0	99	0	0	0
ASCAT	0	100	100	100	100	100	215	215	215	100	215	0	100	0
AVHRR/3	0	0	0	0	0	0	27	27	27	0	27	0	0	0
GOME-2	0	0	0	0	0	0	42	42	42	0	42	0	0	0
GRAS	0	10	10	10	10	10	30	30	30	10	30	0	10	0
HIRS/4	0	0	0	0	0	0	24	24	24	0	24	0	0	0
IASI	0	0	0	0	0	0	210	210	0	0	210	0	0	0
MHS	0	0	0	0	0	0	93	93	93	0	93	0	0	0
S&RSA	0	0	0	0	0	0	86	86	86	0	86	0	0	0
SEM-2	0	0	0	0	0	0	10	10	0	0	10	0	0	0
SVM	306	764.4	764.4	286	389	389	389	727.4	767.4	429	349	867.4	687.4	
EPS	6	6	6	6	9	9	9	9	9	9	9	9	9	9
TTMC	20	20	20	20	120	120	120	120	120	20	160	20	120	120
ADCS	50	388.4	388.4	50	50	50	50	388.4	388.4	50	150	388.4	388.4	
TCS	150	150	150	150	150	150	150	150	150	150	150	150	150	
OBDH	20	60	60	60	60	60	60	60	60	60	60	20	60	20
PS	60	140	140	0	0	0	0	0	0	140	0	0	140	0
PLM	10	145	145	145	550	550	550	550	550	145	550	10	550	10
TOTAL	316	1019.4	1019.4	541	1049	1049	1847	1847	1866.4	1022.4	1887	359	1527.4	697.4

Figure 7.6: Power Budget of MetOp-a

7.3 Positioning of components

The configuration of the solar array in the stowed and deployed and configurations is shown in 7.7. The batteries are placed at the bottom of the propulsion cylinder, between the propellant tanks and a radiator plate. The positioning can be appreciated at the bottom of 7.8.

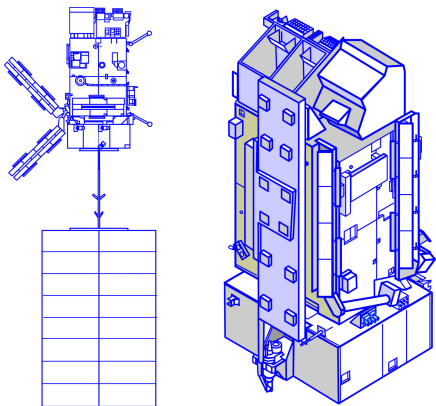


Figure 7.7: Solar Array stowed and deployed configuration

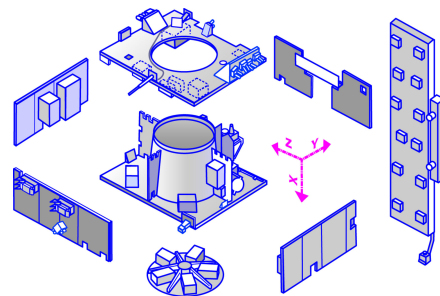


Figure 7.8: Exploded view of service module



8 | Onboard Data Handling Subsystem and Configuration

8.1 Configuration (CONF)

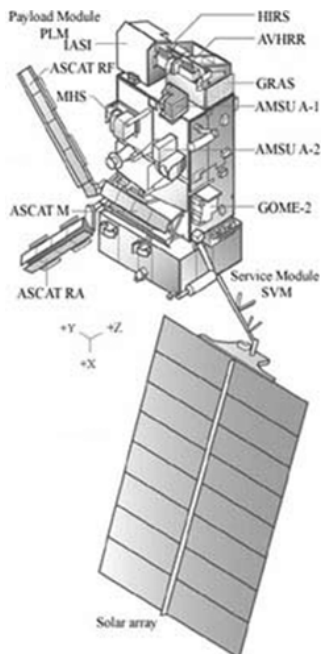


Figure 8.1: MetOp-A service module and payload module

This section provides an overview of the configuration of MetOp-A. This spacecraft consists of three main sections: a solar array, the Service Module (SVM) and Payload Module (PLM) located as shown in figure 8.1. The external configuration of the spacecraft has to meet some expectations in order for the mission to work properly, this part of the design is driven by [54]:

- The Fields Of View (FOV) and performances of instruments, sensors, radiators and antennas
- The available volume under Soyuz-ST Fregat fairing
- The ease and cost of manufacturing, integrating and testing
- The maximum de-coupling among the various elements
- The accessibility to some critical areas (e.g. where required for functional checks of instruments or sensors)

Note that on the next sections, when mentioning the axis of the spacecraft, they will be taken as shown in Figure 8.1.

8.1.1 Launch configuration

As mention before, the launcher used in this mission is the Soyuz-ST Fregat, which is attached to the spacecraft through the SVM. The interface between these two is possible due to the implementation of a standard PAS 1666 MVS adapter, shown in Figure 8.3 [54].

The MetOp-A spacecraft in launch configuration, meaning with all of the appendages retracted, has dimensions of 6.3 m by 2.5 m by 2.5 m [1], with a total mass of 4613 kg (calculated in the propulsion subsystem). The usable volume of the launcher can be appreciated in Figure 8.2. Due to its dimensions it results evident that the spacecraft must be mounted in a vertical position, with the adapter attached to the bottom wider area of the SVM [4].

On the other hand, the correct adapter must be chosen. This specific launcher has three different types of standard payload adapters: the PAS 937 S, the PAS 1666 MVS and the PAS 1194 VS. The first one is qualified to support a payload of 3500 kg, which is far lower than the mass of the spacecraft. While the other two can hold up to 5000 kg [4]. Therefore only two types of adapters could be used for this specific mission. Regarding the other characteristics of these adapters, a trade-off must be done in order to choose the best one between the two remaining. Regarding the PAS 1194 VS this system is the lightest one, with a total mass of 115 kg while the PAS 1666 MVS weights 135kg [4]. However, the PAS 1666 MVS provides a higher clamping tension [4], which, taking into account that the spacecraft needs to lay vertically inside the launcher, is safer for the mission.

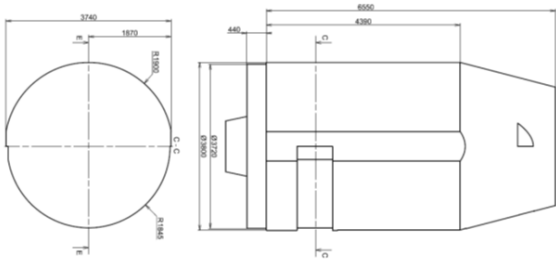


Figure 8.2: Available volume on the launcher [4]

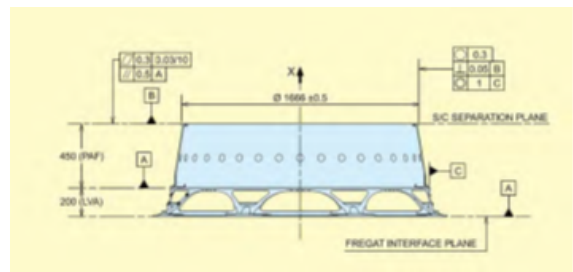


Figure 8.3: Arianespace's PAS 1666 MVS adaptor [4]

Now the last point to review in this section is the positioning of the SVM with respect to the PLM. Since this is a scientific mission, required to provide a lot of data, several instruments must be placed on board, taking most of the available space. For this reason, and since the SVM is almost as heavy as the PLM [1], this first module should be placed at the bottom of the spacecraft (direction +X). This strategic position mitigates the risk of applying extra forces on the payload during the launch phase, which is known to be critical due to the high forces exerted on the spacecraft.

8.1.2 On-orbit configuration

8.1.2.1 Payload Module

Since the MetOp-A mission aims to provide data about meteorological phenomena, the main priority is the PLM, which consists of a total of eleven instruments that must be Nadir pointing during nominal procedures. From a practical point of view, this means that the spacecraft must have a wide flat surface facing at all time to Earth in order to provide constant measurements. At the same time is important to avoid appendages blocking the FOV of the instruments. If we assume to have a rectangular shaped satellite, and since one side must be always Nadir pointing, other instruments can be attached to the other sides pointing as well towards Nadir. Due to the large field of view of the instruments, their relative position to the spacecraft is not important, hence the external placement of the payloads is not relevant as long as they are facing the mentioned direction.

Another constraint found in this module is the thermal control, as there must be enough surface to allow, not only the placement of the instruments, but also of the passive thermal control (radiators) [55]. Out of all the instruments only three depend on the TCS (thermal control subsystem) of the PLM, while the others have their own thermal control. Continuing the assumption of having a rectangular spacecraft, the SVM is occupying one side, and the instruments another two, therefore these are not eligible for the placement of the dissipation devices. So the radiators can be placed on three sides of the spacecraft, on two lateral surfaces (flight and anti-flight, or +Y and -Y) and zenith (+Z).

Considering all these elements, and that one of the drivers of this design is the capacity of having modular grouping of the PLM subsystems for testing, the best shape for the spacecraft, as assumed before, is a rectangle with a wide face pointing always towards Nadir. At the same time, to avoid non desirable torques, specially during launching, it is necessary that the majority of the internal components are placed in a central structure, in this case a cylinder, so the CoM (centre of mass) is centred with respect to the X axis.

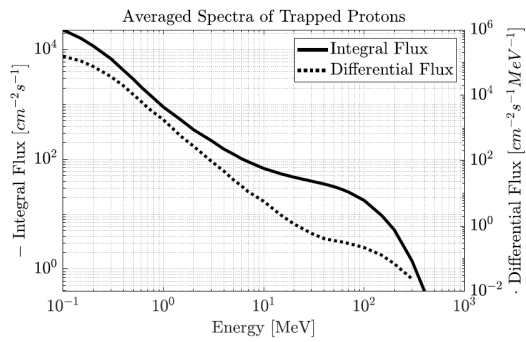


Figure 8.4: Protons [4]

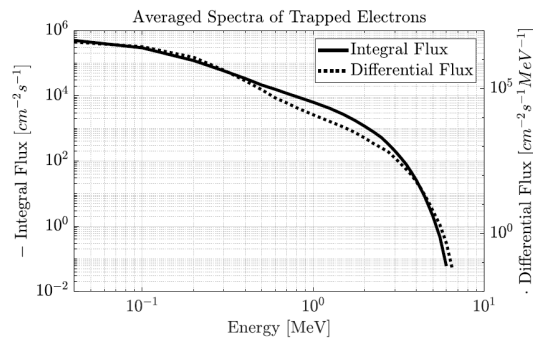


Figure 8.5: Electrons [4]

Another important aspect to take into account is that, being in a low Earth orbit, the satellite is exposed to high fluxes of electrons and protons (see Figures 8.5 8.4) that get trapped in the magnetosphere. Therefore the electronics must be placed inside the central structure to diminish the damages these components can suffer during the mission.

For the TTMTTC, no parabolic antennas are used, so they can be placed on the same face of the instruments (Nadir pointing) without shadowing the fields of view, and providing good communication. For more detailed information check Chapter 4.1.2.3.

8.1.2.2 Service Module

Since this module includes the attitude control subsystem and the power generation [56], it has several requirements in terms of thermal control. Consider that one of the most important components are the batteries, which need to be cooled down effectively in order to work properly and not suffer long term damage, thus a radiator plate must be located as close as possible to the battery pack. In order to satisfy this the best option is to mount it directly on top of it, and thermally insulate it from the rest of the spacecraft [57], for this reason, it has to be placed near one of the SVM's faces.

As mentioned before, this module is in charge of the attitude control. Since the thrusters implemented for the propulsion subsystem are also used for this purpose, their location must be considered. The most important constraint for their placement is that they have to be directed in such a way that the exhaust gases will not damage or contaminate the instruments of the PLM [56].

As a way of having the CoM centred along the X axis, the heavier components have to be positioned in the centre of the module. Therefore, the tanks for the propulsion subsystem as well as the batteries have to be in the centre of the structure. As the batteries need to have the radiator directly on them, the final distribution, from bottom to top, is: adapter, radiator, battery pack, and tanks. This geometry can be appreciated in the figure below (Figure 8.6).

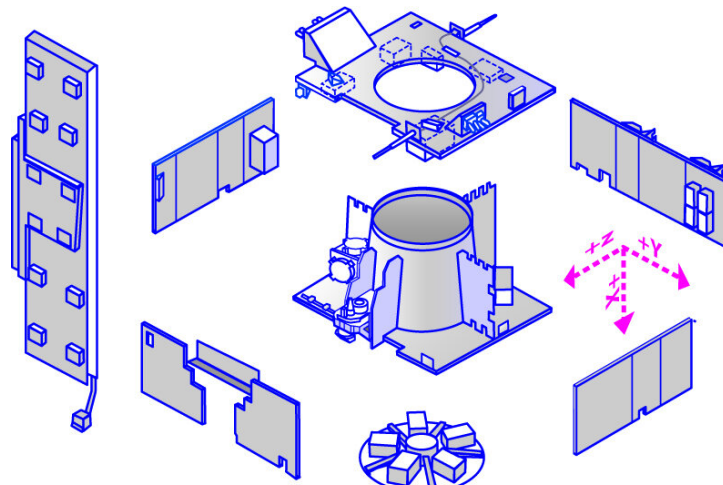


Figure 8.6: Service module



8.1.2.3 Solar array

To ensure the constant visibility of the Earth, the solar panel must be placed either on the opposite side of the spacecraft (Zenith pointing) or as an external appendage. The second choice, even if more difficult to implement since is more complex from the structural point of view, allows to move independently the panels, therefore being able to point towards the Sun whenever needed without compromising the visibility of the instruments.

8.2 On-Board Data Handling (OBDH)

8.2.1 Design

The MetOp-A's OBDH subsystem is mainly driven by the vast amount of data that must be measured and stored, as seen in Chapter 1.7.12. The 11 instruments onboard generate a large amount of information that OBDH must handle in terms of memory and Central Processing Unit (CPU). These are only the requirements coming from the PLM, but it is also necessary to analyze the SVM's expected data.

Regarding ADCS, it has been seen in Chapter 5.3.2 that the satellite uses, during nominal operations, 4 sensors (1 digital Sun sensor, 1 digital Earth sensor, and 2 gyros) and 5 actuators (3 reaction wheels and 2 magnetotorquer). Compared to other similar missions, the data that must be handled is lower as no star sensors are used, making the gyros and the Earth sensor the most challenging in terms of OBDH. From the actuators' side, these two types are the less demanding ones that can be used in this subsystem. Nevertheless, when the control by thrusters takes place, the data generated will be significantly higher as 8 units are required.

ADCS and Operating System (OS) are the two most demanding subsystems as they are the ones generating more code, data and throughput when compared with others. It is expected that they are followed by PS as it also uses 8 thrusters. Finally, as TCS does not have active control and both EPS and TTMTTC are not so challenging, the OBDH requirements are anticipated to be less restrictive [8].

Therefore, the main driver for OBDH design is the great amount of code, data, and throughput generated by the PLM, while the SVM seems less demanding. In fact, considering that the combined data load could be very high, there are two CPUs, one for each module.

8.2.2 Architecture

The MetOp-A's OBDH architecture is divided into SVM and PLM, each one has its own CPU in charge of coordinating and managing all the data. This makes impossible the implementation of a centralized architecture. In fact, everything is distributed following a federated bus structure. Standard OBDH data buses are mounted and used for data exchange between both modules' CPUs [5]. Figures 8.7 and 8.8 show the architecture of both SVM and PLM respectively.

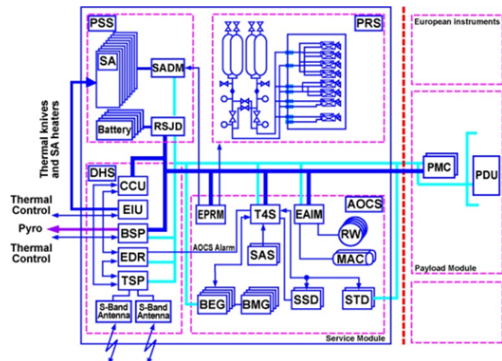


Figure 8.7: Service module OBDH architecture [5]

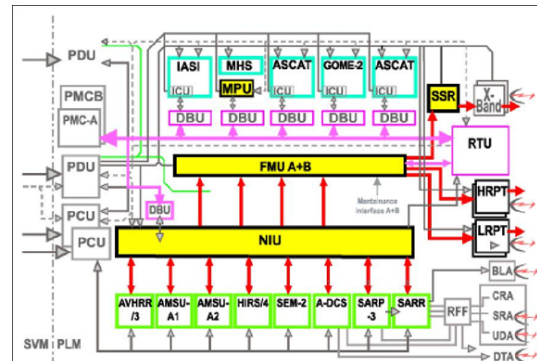


Figure 8.8: Payload module OBDH architecture [1]

8.2.2.1 Service Module

The Central Communication Unit (CCU) is in charge of the SVM data management. It includes a MA31750 microprocessor with a total memory of 448 kwords. Its specifications are introduced in Table 8.1 [5].



Supplier and Computer	Dynex Semiconductor, MA31750
Word Length [bits]	16 [58]
Memory [kwords]	448
Performance [MIPS]	3 [59]

Table 8.1: MA31750 specifications

As it can be seen in Figure 8.7, besides the CCU, there are other units that must be analysed [5]:

- Decoding and reconfiguration unit (EDR). Interfaces with the S-band transponder and oversees telecommand receipt, CCU supervision and Command Pulse Direct Unit (CPDU) telecommand
- Housekeeping and pyrotechnics unit (BSP). Responsible for pyrotechnics commands generation, temperature measurements, actuation of heaters for the SVM and housekeeping of some units inside the SVM
- Electrical Interface Unit (EIU). In charge of the release and deployment of the solar array and TTMTTC for some of the SVM units

8.2.2.2 Payload Module

The PLM data handling functions are performed by:

- CBS (Standard Bus Couplers)
- DBU (Digital Bus Units)
- ICU (Instrument Control Units)
- PMC (Payload Module Computer). Controls all PLM equipment and instruments via an ESA standard OBDH bus
- RBI (Standard Remote Bus Interface ASICs)
- RTU (Remote Terminal Units)

Due to compatibility problems with the NOAA-provided instruments, a dedicated unit, NOAA Interface Unit (NIU), was developed to adapt the American interfaces to European standards. It controls through a dedicated instrument control unit and collects all the data using a Digital Signal Processor (DSP). The Formatting and Multiplexing Unit (FMU), fed by NIU via four distinct data streams, oversees selective encryption. This encryption capability ensures that the measured data is not denied by EUMETSAT or NOAA, creating an adapted encryption to the needs of both entities.

The instruments not provided by NOAA use an ICU in charge of functions such as monitoring of the instrument parameters, preparation of housekeeping telemetry formats or reception and expansion of macro commands [60].

Finally, all the scientific data is acquired as Consultative Committee for Space Data Systems (CCSDS) packets and stored in a solid-state recorder of 24 Gbit [1]. In Chapter 4.1.2.3, the computation which shows that the solid-state recorder memory is enough has already been done.

8.2.3 Reverse Engineering

The reverse engineering approach will be only applied to size the SVM computer as it is the one that can be estimated by similarity. The PLM is specific for each mission, having different tasks, interfaces and components, making it impossible to compute the sizing using statistical approaches.



8.2.3.1 OBC Features

To size the OBDH subsystem, an approach by similarity is used. Based on statistical data [8], the typical code (measured in words), data (measured in words), throughput (measured in KIPS) and frequency (measured in Hz) are retrieved for every component of the satellite. Once this is done, Equation 8.1 is applied to obtain the final throughput value, where $KIPS$ is the number of instructions per second (throughput), f is the acquisition frequency and f_{typ} is the typical frequency coming from statistics.

$$KIPS = \frac{KIPS_{typ} \cdot f}{f_{typ}} \quad (8.1)$$

Table 8.2 shows the components of each subsystem, the units of each one used during operations, the statistical values for the previously mentioned parameters and, finally, the assumed acquisition frequency (f) and the estimated throughput. The units are kept the same as mentioned in the previous paragraph.

The redundant components are not included in the “Number” column as it is assumed that they are in cold redundancy [2]. Special remark has to be highlighted for two specific subsystems:

- PS: each tank is assumed to use one pressure sensor and one control valve
- TTMTTC: as each S-band antenna can be used for both uplink and downlink, it is assumed that each of these operations is performed using both antennas and so 2 transponders. The X-band antenna is the one used by the PLM, which has previously been shown that works separately from the SVM

Regarding the acquisition frequency, it has been mainly chosen through a trade-off between the statistical values and the values used during the work session [8]. This is true for all the components except for:

- Thrusters: the value has been fixed to the minimum impulse bit they can provide [1]
- Sensors: considering the frequency ranges introduced in Chapter 5.3.2, the closest value to the statistical data retrieved is chosen. This has been done for every sensor



ADCS							
Components	Number	Code	Data	KIPS _{typ}	f _{typ}	f	KIPS
RW Control	3	1000.0	300.0	5.0	2.0	2.0	5.0
Thruster Control	8	600.0	400.0	1.2	2.0	8.0	4.8
Magnetic Control	2	1000.0	200.0	1.0	2.0	2.0	1.0
Digital Sun Sensor	1	500.0	100.0	1.0	1.0	1.0	1.0
Digital Earth Sensor	1	1500.0	800.0	12.0	10.0	1.0	1.2
Solar Array Sensor	2	500.0	100.0	1.0	1.0	1.0	1.0
Rate Gyro	2	800.0	500.0	9.0	10.0	40.0	36.0
Kinematic Integration	1	2000	200.0	15.0	10.0	10.0	15.0
Error Determination	1	1000.0	100.0	12.0	10.0	10.0	12.0
Attitude Determination	1	15000.0	3500.0	150.0	10.0	10.0	150.0
Attitude Control	1	24000.0	4200.0	60.0	10.0	10.0	60.0
Complex Ephemeris	1	3500.0	2500.0	4.0	0.5	1.0	8.0
Orbit Propagation	1	13000.0	4000.0	20.0	1.0	1.0	20.0
EPS							
Solar Panel	8	-	-	-	-	-	-
Batteries	5	-	-	-	-	-	-
Cables & Harness	1	-	-	-	-	-	-
Power Voltage Control	1	1200.0	500.0	5.0	1.0	1.0	5.0
Power Current Control	2	1200.0	500.0	5.0	1.0	1.0	5.0
PS							
Tank	4	-	-	-	-	-	-
Thrusters	8	600.0	400.0	1.2	2.0	8.0	4.8
Tank Control Valve	4	800.0	1500.0	3.0	0.1	0.1	3.0
Tank Pressure Sensor	4	800.0	1500.0	3.0	0.1	0.1	3.0
TCS							
Thermal Control	1	800.0	1500.0	3.0	0.1	0.1	3.0
TTMTC							
X-Band Antenna	1	-	-	-	-	-	-
S-Band Antenna	2	-	-	-	-	-	-
LRP Antenna	1	-	-	-	-	-	-
HRP Antenna	1	-	-	-	-	-	-
Transponder (Uplink)	2	1000.0	4000.0	7.0	10.0	10.0	7.0
Transponder (Downlink)	2	1000.0	2500.0	3.0	10.0	10.0	3.0
OS							
I/O Device Handlers	1	2000.0	700.0	50.0	5.0	1.0	10.0
Test and Diagnostics	1	700.0	400.0	0.5	0.1	1.0	5.0
Math Utilities	1	1200.0	200.0	0.5	0.1	1.0	5.0
Executive	1	3500.0	2000.0	60.0	10.0	10.0	60.0
Run Time Kernel	1	8000.0	4000.0	60.0	10.0	10.0	60.0
Complex Autonomy	1	15000.0	10000.0	20.0	10.0	10.0	20.0
Fault Detection (Monitors)	1	4000.0	1000.0	15.0	5.0	1.0	3.0
Fault Correction	1	2000.0	10000.0	5.0	5.0	10.0	10.0

Table 8.2: OBC Features

8.2.3.2 On-Board Memory Size

Once the main OBC features are obtained, it is possible to start the memory sizing. To do so, the Equations 8.2, 8.3, 8.4 and 8.5 are used, where: n_{fun} is the total number of functions; k_{fun} the number of components in each function; $KIPS_{fun}$ the throughput of a single function; WL the Word Length set to 16 bit/word as it is the one of the MA31750; ROM the Read Only Memory; and RAM the Random Access Memory. A 400% margin must be applied to all the computations as it is a very preliminary analysis completely based on statistical data [8].

$$(8.2) \quad Throughput_{tot}[MIPS] = \frac{\sum_{i=1}^{n_{fun}} k_{fun} KIPS_{fun}}{1000} \quad (8.3) \quad Memory_{tot}[kwords] = \frac{Code + Data}{1000}$$

$$(8.4) \quad ROM[MB] = \frac{Code \cdot WL}{8 \cdot 1024^2} \quad (8.5) \quad RAM[MB] = \frac{(Code + Data) \cdot WL}{8 \cdot 1024^2}$$

These computations are done for all the operational modes defined in Chapter 1.7.12, except the Science Transmission mode, which is partially performed by the PLM. The Power Generation mode is also excluded as it



is intrinsic in the others. The difference between modes resides in the active subsystem and in the applied control mode, already defined in Chapter 5.3.2. Nevertheless, the PL subsystem is never included since it is inside the PLM. The features of each operational mode are:

- Science: PS and TTMTTC are switched off and the YSM control mode is used
- Communication: PS is the only subsystem switched off while the YSM control mode keeps being applied. The difference between downlink and uplink is shown in Table 8.2
- Thrusting: TTMTTC is the only non-operative subsystem. OCM control mode is applied in this case and the one for IP manoeuvres is chosen as a worst-case scenario
- Sleep: It is considered to be the same as Science but without the PL active
- Safe: In this case, PS is switched off while TTMTTC is considered active as it is recommendable to always transmit the current status. SFM control is used during Safe operations

The results are introduced and discussed in the following Section 8.2.4

8.2.4 Outputs

The memory size results are shown in Table 8.3

Mode	ROM [Mb]	RAM [Mb]	Memory [kwords]	Throughput [MIPS]
Science	1.018	1.480	776	2.711
Uplink	1.037	1.575	826	2.781
Downlink	1.037	1.547	811	2.741
Thrusting	1.113	1.732	908	3.129
Sleep	1.018	1.480	776	2.711
Safe	1.025	1.547	811	2.847

Table 8.3: Memory sizing

Clearly, the most demanding operational mode in terms of data handling is the Thrusting mode. This is caused by the use of the PS subsystem, which includes 8 thrusters and 4 valves and pressure sensors. Combined with this, the OCM control law uses 1 digital Sun sensor, 1 digital Earth sensor and 2 gyros for attitude determination, which is the most demanding sensor configuration inside all the control laws. It is followed by the operations having TTMTTC subsystem active, as it supposes extra information that must be managed and stored with respect to the Science mode. It can be noticed that Safe is slightly less demanding than Communication as it uses only 2 Sun array sensors. Inside Communication mode, the uplink is a bit more challenging than the downlink. Finally, both Science and Sleep have identical values as they have the same characteristics, as previously said. They are the less demanding modes for the OBDH subsystem.

At last, when compared with the values in Table 8.1, it seems that the OBC selected for the mission is not capable of answering the requirements even though the throughput values are slightly higher than the maximum admissible. This can be caused by the very preliminary nature of this analysis and the extra 400% added during the computations.



Bibliography

- [1] ESA. EoPortal — MetOp (Meteorological Operational Satellite Program of Europe).
- [2] Yoke T. Yoon and Pier Luigi Righetti. *Precise Calibration Of Multi-segment Maneuvers For Eumetsat Polar System (Eps) Operations Planning*, 2015.
- [3] P.G Edwards and D Pawlak. Metop: The Space Segment for Eumetsat's Polar System, 2000.
- [4] Arianespace. *Soyuz User's Manual*, march 2012.
- [5] ESA. Service Module data handling.
- [6] K. Merz, M. A. Martín Serrano, D. Kuijper, and M.A. García Matatoros. *The Metop-a Orbit Acquisition Strategy And Its Leop Operational Experience*, 2007.
- [7] Gilmore David G. *Spacecraft Thermal Control Handbook*. The Aerospace Press, 2 edition, 2002.
- [8] M. R. Lavagna. SSEO course slides at Politecnico di Milano, 2023.
- [9] Spoto François, Bordes Yves, Chalkley Simon, Huertas Luis, Sy Omar, Buhler Yves, and Caujolle Jean-Michel. *Preparing MetOp For Work: Launch, Early, Operations and Commissioning*, 2006.
- [10] EUMETSAT. *ATOVS Level 1b Product Guide*, January 2010.
- [11] ESA. AMSU-A1 components.
- [12] ESA. About AVHRR/3.
- [13] NOAA. AVHRR.
- [14] ESA. About MHS.
- [15] EUMETSAT. SEM-2.
- [16] NOAA. SARSAT.
- [17] P. Righetti, Jose M.J. Gamo, and Richard Dyer. *Mission Analysis Of Metop-a End-of-life Operations*, 2014.
- [18] Ariane Group. 1n, 20n, 400n and heritage thruster - chemical monopropellant thruster family.
- [19] Antimo Damiano, Pier Luigi Righetti, and Anders Soerensen. *Operational Local Time and Eccentricity Management for Metop-A*, 2009.
- [20] Lazaro D. Sancho F. and Righetti P.L. *Out-of-plane manoeuvre campaigns for Metop-A: planning, modelling, calibration*, 2009.
- [21] SRE-PA & D-TEC staff. *Margin philosophy for science assessment studies*, 2012.
- [22] Wertz James R., Everett David F., and Puschell Jeffery J. *The New SMAD*. Microcosm Press, 2 edition, 2015.
- [23] EUMETSAT. EPS-SG (Metop-SG) Direct Data Broadcast (DDB) Radio Frequency (RF) Space to Ground Interface Control Document (ICD).
- [24] ESA. Kiruna station, 2023.
- [25] James Richard Wertz. 13, 2003.
- [26] Wikimapia. Svalsat satellite ground station, 2013.
- [27] L3harris. As-48915 series omnidirectional conical spiral antenna.



- [28] OSCAR. Satellite: Metop-a.
- [29] ESA. *Esrangle User's Handbook - Launch Range Instrumentation*, 2022.
- [30] Wei Zhou, Lilong Liu, Liangke Huang, Yibin Yao, Jun Chen, and Songqing Li. *A New GPS SNR-based Combination Approach for Land Surface Snow Depth Monitoring*, 2019.
- [31] James Richard Wertz. 13, 2003.
- [32] ESA. Service Module attitude and orbit control (including propulsion).
- [33] P. A. Dubock, F. Spoto, J. Simpson, D. Spencer, E. Schutte, and H. Sontag. *The Envisat satellite and its integration*, June 2001.
- [34] EUMETSAT. *EUMETSAT Polar System: EPS Mission Conventions Document*, 2005.
- [35] Eric Arnaud, Jeremy Dugenet, Kevin Elis, Arnaud Girardot, Davy Guihard, Cyrille Menudier, Thierry Monediere, Fanny Roziere, and Marc Thevenot. *Compact Isoflux X-Band Payload Telemetry Antenna With Simultaneous Dual Circular Polarization for LEO Satellite Applications*, 2020.
- [36] ESA. TNO Coarse Sun Sensor using European cells.
- [37] Barre, Hubert and Betto, Maurizio and Mason, Graeme and Marcille, Hervé and Pendaries, Michel and Fayard, René and Huchler, Markus. MetOp Second Generation System overview.
- [38] Kongsberg. KARMA-5 SG Solar Array Drive Mechanism.
- [39] NASA. *Spacecraft magnetic torques*, march 1969.
- [40] S. Pessina, N.M.G. Gomes Paulino, J.M. De Juana, and P. Righetti. *EUMETSAT study for attitude dynamics and disturbances in LEO and GEO environments*, 2014.
- [41] Franco Bernelli Zazzera. *Lecture Notes Spacecraft Attitude Dynamics*, 2022 - 2023.
- [42] C.W. de Boom and N. van der Heiden. *A novel digital sun sensor: development and qualification for flight*, october 2003.
- [43] E.J. van der Heide, R. Ferreira, P. van Put, and P. Le. *Reaction wheels at Bradford Engineering*, june 2011.
- [44] Jim Krebs and Eric Stromswold. *High Efficiency Magnetic Torquer Bars*, february 2014.
- [45] Dolce Silvio, Faust Thomas, Schilke Jürgen, and Peabody Hume. *Lessons Learned from the METOP Thermal Analysis and Testing*, 2003.
- [46] Dolce Silvio, Faust Thomas, and Schilke Jürgen. *METOP PLM Thermal Balance and Thermal Vacuum Test*, 2003.
- [47] ESA. Electrical power.
- [48] K.A. Munzer, K.T. Holdermann, R.E. Schlosser, and S. Sterk. *Thin monocrystalline silicon solar cells*, 1999.
- [49] Richard Dyer, Pier Luigi Righetti, Carlos Vera, and Sylvain Vey. *Metop-A Mission Extension: Surviving on a drifting LTAN*, 2018.
- [50] Vincent Lempereur.
- [51] T Pipoli, B Hendel, G Dudley, and M Schautz. *Evaluation of Maximum Safe Voltage for Nickel-Cadmium Cells*.
- [52] Michèle Lavagna. Eletrical power subsystem.
- [53] ESA. Metop poised for launch - bulletin - space for europe, August 2006.



- [54] ESA. Spacecraft specifications.
- [55] ESA. Payload Module.
- [56] ESA. Service Module.
- [57] ESA. Service Module thermal control.
- [58] Dynex Semiconductor. *MA31750 High Performance MIL-STD-1750 Microprocessor*, 2002. Datasheet.
- [59] M.S. Gorbunov. *Design of fault-tolerant microprocessors for space applications*, 2019. Space Flight Safety-2018.
- [60] ESA. GOME-2 control and data handling system.